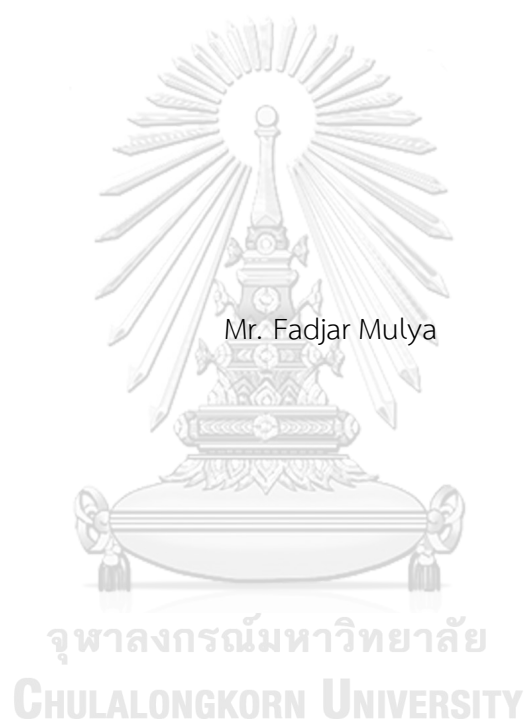


THEORETICAL STUDY OF LITHIUM ABSORPTION IN SILICON NANOSTRUCTURES FOR
APPLICATION AS ANODES IN LITHIUM-ION BATTERIES



A Dissertation Submitted in Partial Fulfillment of the Requirements
for the Degree of Doctor of Philosophy in Chemistry
Department of Chemistry
FACULTY OF SCIENCE
Chulalongkorn University
Academic Year 2022
Copyright of Chulalongkorn University

การศึกษาเชิงทฤษฎีของการดูดซึมลิเทียมในโครงสร้างนาโนซิลิคอนสำหรับการประยุกต์เป็นแอโนดใน
แบตเตอรี่ลิเทียมไอออน



วิทยานิพนธ์นี้เป็นส่วนหนึ่งของการศึกษาตามหลักสูตรปริญญาวิทยาศาสตรดุษฎีบัณฑิต
สาขาวิชาเคมี ภาควิชาเคมี
คณะวิทยาศาสตร์ จุฬาลงกรณ์มหาวิทยาลัย
ปีการศึกษา 2565
ลิขสิทธิ์ของจุฬาลงกรณ์มหาวิทยาลัย

Thesis Title THEORETICAL STUDY OF LITHIUM ABSORPTION IN
SILICON NANOSTRUCTURES FOR APPLICATION AS
ANODES IN LITHIUM-ION BATTERIES

By Mr. Fadjar Mulya

Field of Study Chemistry

Thesis Advisor Professor Dr. VUDHICHAJ PARASUK

Accepted by the FACULTY OF SCIENCE, Chulalongkorn University in Partial
Fulfillment of the Requirement for the Doctor of Philosophy

..... Dean of the FACULTY OF SCIENCE
(POLKIT SANGVANICH)

DISSERTATION COMMITTEE

..... Chairman
(Dr. Supawadee Namuangruk)

..... Thesis Advisor
(Professor Dr. VUDHICHAJ PARASUK)

..... Examiner
(Professor Dr. THAWATCHAI TUNTULANI)

..... Examiner
(Associate Professor Dr. SOAMWADEE
CHAIANANSUTCHARIT)

..... Examiner
(Assistant Professor Dr. SAKULSUK UNARUNOTAI)

พัตจารย์ มุลยา : การศึกษาเชิงทฤษฎีของการดูดซึมลิเทียมในโครงสร้างนาโนซิลิคอน
 สำหรับการประยุกต์เป็นแอโนดในแบตเตอรี่ลิเทียมไอออน. (THEORETICAL STUDY
 OF LITHIUM ABSORPTION IN SILICON NANOSTRUCTURES FOR APPLICATION
 AS ANODES IN LITHIUM-ION BATTERIES) อ.ที่ปรึกษาหลัก : วุฒิชัย พาราสุข

การซึมซับและการดูดซับของลิเทียมในโครงสร้างซิลิคอนขนาดเล็ก : ซิลิคอนควอนตัมดอท (SiQDs), ซิลิคอนนาโนไวร์ (SiNWs) และ ซิลิคอนนาโนพอร์ (SiNPs) ได้ศึกษาโดยใช้ทฤษฎีฟังก์ชันนอลความหนาแน่น (DFT) โดยใช้ฟังก์ชันไฮบริด M06-2X และเบซิสเซต 6-31G+(d) โดยตำแหน่งที่มีลักษณะเป็นพีระมิดทั้ง Td_{inner} และ $Td_{surface}$ เป็นตำแหน่งที่เหมาะสมที่สุดสำหรับการดูดซับลิเทียมเนื่องจากมีพลังงานยึดเหนี่ยวที่เหมาะสม สำหรับการซึมซับและการดูดซับลิเทียมเดี่ยว ซิลิคอนควอนตัมดอทมีพลังงานยึดเหนี่ยว 1 eV ซิลิคอนนาโนไวร์มีพลังงานยึดเหนี่ยว 1.28 eV และ ซิลิคอนนาโนพอร์มีพลังงานยึดเหนี่ยว 0.73 eV สำหรับการดูดซับลิเทียมหลายตัวมีลักษณะคล้ายคลึงกันคือมีพลังงานงานยึดเหนี่ยว 1.12 eV สำหรับ SiQD, 1.21 eV สำหรับ SiNW และ 0.94 eV สำหรับ SiNP การคำนวณปริมาตรโมเลกุลเพื่อประเมินการขยายตัวของโมเลกุลพบว่าการเปลี่ยนแปลงปริมาตรไม่เกิน 2.51% และไม่แปรผันตามจำนวนอะตอมของลิเทียมแต่ขึ้นอยู่กับตำแหน่งการดูดซึมและดูดซับ โดยช่องว่างระหว่างแถบพลังงานของโครงสร้างซิลิคอนขนาดเล็กขึ้นอยู่กับขนาดและการทำปฏิกิริยากับลิเทียม ซึ่งถ้าโครงสร้างมีขนาดใหญ่จะทำให้การนำไฟฟ้าได้ดีขึ้น ดังนั้นโครงสร้างนาโนซิลิคอนขนาดใหญ่เหมาะสำหรับใช้เป็นวัสดุขั้วแอโนดของแบตเตอรี่ลิเทียมไอออน เนื่องจากวัสดุดังกล่าวสามารถให้ความหนาแน่นของพลังงานสูงและมีการขยายตัวในปริมาณเล็กน้อยโดยมีค่าการนำไฟฟ้าที่เหมาะสม

สาขาวิชา เคมี
 ปีการศึกษา 2565

ลายมือชื่อนิสิต
 ลายมือชื่อ อ.ที่ปรึกษาหลัก

6273024023 : MAJOR CHEMISTRY

KEYWORD: DFT, Lithium-ion battery, Absorption, Molecular Volume

Fadjar Mulya : THEORETICAL STUDY OF LITHIUM ABSORPTION IN SILICON NANOSTRUCTURES FOR APPLICATION AS ANODES IN LITHIUM-ION BATTERIES. Advisor: Prof. Dr. VUDHICHAJ PARASUK

The absorption and adsorption of lithium in silicon nanostructures: silicon quantum dots (SiQDs), silicon nanowires (SiNWs) and silicon nanopores (SiNPs) were studied using density functional theory (DFT) with M06-2X hybrid functional and 6-31G+(d) basis set. The tetrahedral sites, both Td_{inner} and $Td_{surface}$, are the most preferred sites for lithiation due to their favorable binding energy profiles. For single lithium absorption and adsorption, SiQDs exhibit a binding energy of 1 eV, SiNWs demonstrate a binding energy of 1.28 eV, and SiNPs display a binding energy of 0.73 eV. Similarly, multiple lithium adsorptions yield binding energies of 1.12 eV for SiQDs, 1.21 eV for SiNWs, and 0.94 eV for SiNPs. The binding energy is altered more with the adsorption site, than with the cluster size. Molecular volume had been calculated to assess the volume expansion. A volume change of no greater than 2.51% was observed and it does not vary with the number of Li atoms, but depends on the absorption and adsorption sites. The energy gap of silicon nanostructures depends on the size (the larger being more conductive) and lithiation. Thus, large-sized silicon nanostructures are recommended for anode materials of Li-ion batteries, since the materials can yield high energy density and have small volume expansion with reasonable conductivity.

Field of Study: Chemistry

Student's Signature

Academic Year: 2022

Advisor's Signature

ACKNOWLEDGEMENTS

I would like to express my sincere gratitude to my advisor, Prof. Dr. Vudhichai Parasuk, for his invaluable advice, suggestions, and encouragement throughout my study. I am also deeply thankful to Prof. Dr. Thawatchai Tuntulani, Assoc. Prof. Dr. Soamwadee Chaianansutcharit, Asst. Prof. Dr. Sakulsuk Unarunotai, and Dr. Supawadee Namuangruk, the members of my thesis committee, for their insightful suggestions and guidance.

I am immensely grateful to the following institutions for providing the essential research facilities: the Center of Excellence in Computational Chemistry (CECC) at the Department of Chemistry, Faculty of Science, Chulalongkorn University; the National Electronics and Computer Technology Center (NECTEC) through the National e-Science Consortium; and the NSTDA Supercomputer Center (ThaiSC).

I would like to acknowledge the Graduate Scholarship Programme for ASEAN or Non-ASEAN Countries, Chulalongkorn University, and The Southeast Asia-Europe Joint Funding Scheme for Research and Innovation (JFS) for their financial support.

I would also like to express my heartfelt appreciation to my family, especially my wife, Valya Nurfadila, and my parents, for their unwavering support and love. I dedicate this work to the memory of my beloved mother, Ibu Marnis, who showered me with a lifetime of love.

Fadjar Mulya

TABLE OF CONTENTS

	Page
.....	iii
ABSTRACT (THAI).....	iii
.....	iv
ABSTRACT (ENGLISH).....	iv
ACKNOWLEDGEMENTS.....	v
TABLE OF CONTENTS.....	vi
LIST OF TABLES.....	viii
LIST OF FIGURES.....	ix
CHAPTER I INTRODUCTION.....	1
1.1 OVERVIEW.....	1
1.2 RESEARCH OBJECTIVES.....	4
CHAPTER II THEORETICAL BACKGROUND.....	5
2.1 QUANTUM CHEMISTRY.....	5
2.1.1. The Schrödinger equation.....	5
2.1.2. Born-Oppenheimer approximation.....	7
2.1.3. Hartree-fock (HF) approximation.....	7
2.1.4. Density functional theory.....	9
2.1.5. Basis set.....	13
2.2 RECHARGEABLE LITHIUM-ION BATTERY.....	14
CHAPTER III DETAILS OF THE CALCULATION.....	16
3.1 LITHIUM ABSORPTION ON BULK SILICON.....	16

3.2 LITHIUM ABSORPTION AND ADSORPTION ON SILICON QUANTUM DOTS.....	16
3.3 LITHIUM ABSORPTION AND ADSORPTION ON SILICON NANOWIRES AND NANOPORES.....	18
CHAPTER IV RESULTS AND DISCUSSION	21
4.1 LITHIUM ABSORPTION ON BULK SILICON.....	21
4.1.1 Binding of Li to silicon bulk and volume expansion.....	21
4.1.2 Effect of Li absorption on the band gap of silicon.....	22
4.2 LITHIUM ABSORPTION AND ADSORPTION ON SILICON QUANTUM DOTS.....	24
4.2.1 Binding of Li to SiQDs.....	24
4.2.2 Effect of Li absorption and adsorption on the volume expansion	28
4.2.3 Effect of Li absorption and adsorption on the energy gap	31
4.3 LITHIUM ABSORPTION AND ADSORPTION ON SILICON NANOWIRE AND NANOPORE.....	36
4.3.1 Binding of Li to SiNWs with diameters of 1 nm, 1.5 nm, and 2 nm	36
4.3.2 Effect of Li absorption, adsorption, and porosity on the energy gap.....	37
4.3.3 Effect of Li absorption and adsorption on the volume expansion	39
CHAPTER V CONCLUSION	41
REFERENCES.....	43
VITA.....	58

LIST OF TABLES

	Page
Table 1. Binding energy per Li adsorption (E_{bind}), the change of molecular volume (ΔMV), and the band gap energy (E_g) of Li-Si bulk structures.	21
Table 2. The 43 structures of the absorption and adsorption complex of Li-SiQDs ...	25
Table 3. Binding energy (E_{bind}) of single and multiple Li adsorption on SiQDs.....	26
Table 4. Energy gaps (E_g) of various sizes of SiQDs and nLi-SiQDs.....	31
Table 5. Binding energy (E_{bind}) and energy gap (E_g) of Li absorption and adsorption on SiNWs and SiNPs.....	36
Table 6. Binding energy (E_{bind}) and energy gap (E_g) of multiple Li adsorptions on SiNWs and SiNPs.....	38

LIST OF FIGURES

	Page
Figure 1. Jacob’s ladder diagram of DFT hybrid functionals.	12
Figure 2. A schematic drawing illustrating the mechanism of rechargeable Li-ion batteries during the discharge and charge processes.....	14
Figure 3. The structure of (a) bulk silicon with two absorption sites: (b) Tetrahedral and (c) Hexagonal.....	16
Figure 4. Ten models of silicon quantum dots (SiQDs).....	17
Figure 5. Two absorption sites, (a) Tetrahedral and (b) Hexagonal and three adsorption sites (c) hollow, (d) bridge and (e) on-top.....	17
Figure 6. The surface of silicon nanowires with diameter of (a) 1 nm, (b) 1.5 nm and (c) 2 nm.....	18
Figure 7. The structure of (a) silicon nanowires/SiNWs and (b) porous silicon nanowires/SiNPs with a diameter of 1 nm (top view) and length of 0.5 nm (side view).	19
Figure 8. Band gap and DOS profile of (a) Bulk structures of silicon with two absorption sites: (b) Td and (c) Hex.....	23
Figure 9. Binding energy of single Li for three sites: Td _{inner} , Td _{surface} , and Hex.....	25
Figure 10. The percentage change in molecular volume of SiQDs after Li adsorption	29
Figure 11. Energy gaps of various sizes of un-adsorbed and nLi-adsorbed SiQDs.....	32
Figure 12. HOMO, LUMO energies (eV) of SiQDs, (a) single and (b) multiple Li adsorbed on SiQDs (Li-SiQDs and nLi-SiQDs).....	33
Figure 13. Binding energy of Li-SiNWs and Li-SiNPs.....	37
Figure 14. The percentage change in molecular volume of SiNWs and SiNPs after Li adsorption.....	40

CHAPTER I

INTRODUCTION

1.1 OVERVIEW

Lithium-ion (Li-ion) batteries are widely utilized as power source across a broad spectrum of applications due to their high energy density, high coulombic efficiencies long cycle, fast charging, and environment friendly which makes it the preferred technology for portable electronic devices, power tools, and electric vehicles. The adoption of Li-ion batteries in a majority of transportation systems, in place of gasoline, would result in a significant decrease in greenhouse gas emissions [1-6]. In the past, the most commercialized lithium-ion batteries use graphite-based anodes which have theoretical capacities of less than 200 mAh/g. To extend the application of Li-ion batteries such as in electric vehicles and power tools, its required high capacities of batteries (> 200 mAh/g) [7-11]. Silicon-based electrodes can be proposed to achieve high capacities of battery due to their high capacity of 4200 mA h/g which is 10 times larger than graphite. Furthermore, silicon is non-toxic, low-cost, and high-abundance element [12, 13]. However, silicon anodes have several challenges to tackle such as changes in volume during intercalation, low electronic conductivity, and slow lithium diffusion [10, 14-16]. Addressing these challenges can be accomplished through precise manipulation of the geometric arrangement and fabrication of minute porous silicon structures, including nanopores. [17-19]. Thus, it is our interest to study the lithium absorption and adsorption on low dimensional silicon nanostructures such as silicon quantum dots (SiQDs), silicon nanowires (SiNWs), and silicon nanopores (SiNPs). The knowledge obtained in this study will lead to the development of high-energy-density lithium-ion rechargeable batteries.

The fundamental process governing the charging and discharging of lithium-ion batteries revolves around the absorption and adsorption of lithium atoms/ions onto the surface of the anode materials. Using DFT calculation, several studies observed

the absorption and adsorption of lithium on graphene and silicon surface. Harismah et al. [20] using B3LYP hybrid functional and Pattaraongdilok and Parasuk using M06-2X [21] investigated the adsorption of lithium atom/ion on graphene quantum dots (GQDs) surface. They agreed that Li and Li^+ prefer to adsorb on the central of GQDs at the hollow site of the hexagonal carbon ring. While Zheng et al. [22] performed the calculation on the GGA level to study the lithium insertion and absorption on the graphene sheets. They reported that Li^+ was absorbed on the center of the carbon ring, and some charge transfers worked from Li^+ ion to the graphene surface. Moreover, Wan et al. [23] explained the lithium insertion on bulk silicon which has two main insertion sites: tetrahedral and hexagonal. Tritsaris performed calculations with PBE level to observe the diffusion of lithium in a bulk amorphous silicon [24] and a layered silicon (silicene) surface [25]. For bulk amorphous silicon, they reported that energy barriers for the diffusion are only one of the factors that control the diffusion process while layered silicon has a smaller structural change during lithiation and delithiation and lower volume change (<25%) compare with crystalline silicon. Xu et al. [26] investigated the adsorption of lithium on single-layer silicene using the PBE level of calculation. They noticed that hollow is the most stable site and the van der Waals effect does not play a crucial role in Li and silicene, unlike the interaction between Li and graphene.

SiQDs, or silicon quantum dots, refer to silicon semiconductors with sizes ranging from 1 to 10 nm [27, 28]. These nanoscale structures hold immense potential for various applications in electronic and optical devices at the nanoscale level [29, 30]. By reducing the size of silicon nanomaterial to the scale of quantum dots, a notable enhancement in electrochemical performance can be achieved [31, 32]. Additionally, SiQDs exhibit short lithium diffusion distances, which contribute to enhanced battery rates and cycling performances. In their study, Aghajamali et al. [31] investigated the electrochemical properties of various nanocomposites consisting of Si crystals with different sizes: 3 nm, 5 nm, 8 nm, and 15 nm. They observed that reducing

the size from 15 nm to 3 nm significantly improved the cycling stability of the annealed Si nanocrystals composite, primarily due to enhanced stress/strain tolerance. Furthermore, Choi et al. [32] proposed the utilization of π -conjugated molecule bridged SiQDs clusters as anode materials, which exhibit enhanced electrochemical performance by modifying the organic structures and introducing different functional groups. These findings suggest that SiQDs can serve as a representative model for silicon nanostructures as anodes in lithium-ion batteries, offering promising potential for improved battery performance.

SiNWs are one-dimensional nanomaterial that is grown directly on the metallic current collector substrate. The geometry of SiNWs gives several advantages such as: allowing for better accommodation of the large volume changes without fracture, connecting electrically to the metallic current collector (contributing to the capacity), and having direct 1D electronic pathways for efficient charge transport [33-35]. This model is used by several researchers to study the absorption/diffusion of lithium with DFT calculation. Zhang et al. [36] using the GGA level of calculation investigated single Li atom insertion in various types of SiNWs with different diameters, growth directions, and three model insertion sites. They concluded that Li binding energy increases as the diameter grows and the surface site is the highest binding energy while the intermediate is the lowest. Salazar et al. [37] performed DFT calculation with LDA function to study the mechanical and electronic properties of SiNWs, Young's modulus, and energy gap as a main parameter to show the effect of surface passivation of SiNW. In summary, it is possible to simultaneously control the energy gap and Young's modulus by tuning the Li concentration on the surface of SiNWs. Also, Santiago et al. [38] with LDA function reported two model absorptions of lithium on SiNW (lithiation): surface and interstitial. They presented the effects of surface and interstitial Li atoms on the electronic and mechanical properties of hydrogen-passivated SiNWs.

SiNPs have emerged as a promising material for the development of nano anodes in lithium-ion batteries. These nanopores exhibit unique properties such as

high surface area, enhanced electronic conductivity, and the ability to accommodate large volumes of lithium ions. As a result, they offer the potential to significantly improve the performance of lithium-ion batteries, which have become ubiquitous in a wide range of applications from portable electronics to electric vehicles [39-42]. Zhu et al. [43] showed the SiNP anode with 80% porosity that has a high specific capacity (2570 mAh/g) and good cycling performance (>200 cycles) without any electrolyte additives. Gonzalez et al. [44] that performed DFT calculation with PBE functional reported the absorption of lithium on the porous silicon, it has three model absorption sites: tetrahedral-inner, hexagonal, and tetrahedra-surfaces. Thus, SiNPs can be a promising, higher-capacity alternative for anodes of lithium-ion batteries.

In this work, we try to model and simulate the absorption and adsorption of lithium on silicon nanostructures e.g., SiQDs, SiNWs, and SiNPs for application as anodes in lithium-ion batteries. Binding energy, molecular volume, and energy gap will be reported in this study. This knowledge would help us to design materials for the silicon anode of Li-ion batteries with better capacity and cycle life.

1.2 RESEARCH OBJECTIVES

In this study, the effects of lithium absorptions and adsorption on the molecular and electronic structures of silicon nanostructures e.g., SiQDs, SiNWs, and SiNPs were investigated. In addition, this knowledge would help us to design materials for the silicon anode of Li-ion batteries with better capacity and cycle life.

CHAPTER II

THEORETICAL BACKGROUND

2.1 QUANTUM CHEMISTRY

Quantum chemistry is based on the principles of quantum mechanics to solve the problem in chemistry. It can be used to describe microscopic phenomena such as the behavior of electrons in atoms and molecules. These states are described by a mathematical function called a wave function which contains all the information that can be known about the system, such as its position, momentum, and energy. The wave function not only describes the location of the electrons but also the probability of finding them in that location. In quantum chemistry, we use the Schrödinger equation to solve the wave function and calculate the behavior of electrons in a system. There are many applications of quantum calculations in chemistry such as thermodynamic properties, spectroscopy, molecular properties, transition states in chemical reactions, stability of molecules, reaction intermediate, and mechanism of chemical reaction [45].

2.1.1. The Schrödinger equation

Schrödinger equation [46, 47] is a second-order differential equation. The equation was formulated by Erwin Schrodinger, an Austrian physicist, who was awarded the Nobel Prize in Physics in 1933 for the discovery of new productive forms of atomic theory.

The Schrödinger equation can be characterized as follows:

$$\hat{H}\Psi = E\Psi \quad (2.1)$$

In this context, the Schrödinger equation is defined in terms of the following variables:

H represents the Hamiltonian operator,

Ψ represents the wave function, and

E represents the energy associated with the state.

The comprehensive expression for the total Hamiltonian of a molecular system, represented in atomic units, can be stated as follows:

$$\mathbf{H} = \mathbf{T}_N + \mathbf{T}_e + \mathbf{V}_{Ne} + \mathbf{V}_{ee} + \mathbf{V}_{NN} \quad (2.2)$$

where, \mathbf{T}_N = nuclear kinetic term,

$$= \sum_A -\frac{1}{2M_A} \nabla_A^2,$$

\mathbf{T}_e = electron kinetic term,

$$= \sum_i -\frac{1}{2} \nabla_i^2,$$

\mathbf{V}_{Ne} = electron-nuclear attraction term,

$$= \sum_A \sum_i \frac{Z_A}{|\vec{R}_A - \vec{r}_i|},$$

\mathbf{V}_{ee} = electron-electron repulsion term,

$$= \sum_{i < j} |\vec{r}_i - \vec{r}_j|^{-1}$$

and \mathbf{V}_{NN} = nuclear-nuclear repulsion term,

$$= \sum_{A < B} \frac{Z_A Z_B}{|\vec{R}_A - \vec{R}_B|}.$$

2.1.2. Born-Oppenheimer approximation

Because of the considerable complexity associated with solving the Schrödinger equation in scenarios involving multiple dimensions, it can become extremely challenging. To alleviate this complexity, the Born-Oppenheimer approximation is frequently utilized. This approximation assumes that the movement of atomic nuclei and electrons can be treated independently, resulting in a simplification of the problem. Consequently,

$$H_{elec} = T_e + V_{Ne} + V_{ee} \quad (2.3)$$

and

$$H_{elec} \Psi_{elec}(\vec{r}; \vec{R}) = E_{elec} \Psi_{elec}(\vec{r}; \vec{R}) \quad (2.4)$$

The electronic wave function, denoted as $\Psi_{elec}(\vec{r}, \vec{R})$, represents a function that depends on both the nuclear and electronic coordinates (\vec{r}). The energy associated with the electronic component is represented as E_{elec} and is parameterized by the molecular coordinate (\vec{r}). Consequently, the total energy, E_{total} is determined by these factors.

$$E_{total} = E_{elec} + V_{NN} \quad (2.5)$$

2.1.3. Hartree-fock (HF) approximation

The Hartree-Fock approximation [48] is used to solve the Schrödinger equation for many-electron systems specifically in terms of the electron-electron repulsion term (V_{ee}) which is impossible to get the exact solution for (equation 2.3).

In the Hartree-Fock approximation, the wave function for a molecule is described as a product of single-electron wave functions, known as orbitals. These orbitals are calculated using the Schrödinger equation, but the interaction between electrons is treated in a simplified way. This method allows for fast and efficient

calculations of the electronic structure of molecules, making it a popular tool in quantum chemistry.

The interaction between electrons is simplified by the mean-field approximation, which approximates the electron-electron repulsion. As a result, the Hartree-Fock energy E_{HF} can be expressed mathematically:

$$E_{HF} = \langle \Psi_0 | H_{el} | \Psi_0 \rangle \quad (2.6)$$

Ψ_0 is the HF wave functions or the Slater determinant

$$= \frac{1}{\sqrt{N!}} \begin{vmatrix} \chi_1(\vec{x}_1) & \chi_2(\vec{x}_1) & \dots & \chi_N(\vec{x}_1) \\ \chi_1(\vec{x}_2) & \chi_2(\vec{x}_2) & \dots & \chi_N(\vec{x}_2) \\ \vdots & \vdots & \ddots & \vdots \\ \chi_1(\vec{x}_N) & \chi_2(\vec{x}_N) & \dots & \chi_N(\vec{x}_N) \end{vmatrix} \quad (2.7)$$

where $\chi_j(\vec{x}_1) = \text{molecular orbital} = \chi_j(\vec{r}_i, \vec{w}_i)$

$\vec{x}_i = \text{spatial-spin coordinate}$

$\vec{r}_i = \text{spatial coordinate}$

$\vec{w}_i = \text{spin coordinate}$

$\chi_j(\vec{x}_1)$ can be obtained through the Fock equation below:

$$\hat{f} \chi_i = \varepsilon_i \chi_i, \quad i = 1, 2, \dots, N \quad (2.8)$$

where \hat{f} is the Fock operator and ε_i is the orbital energy.

In which,

$$\begin{aligned} \hat{f} &= -\frac{1}{2} \nabla_i^2 - \sum_A \frac{Z_A}{r_{iA}} + V_{HF}(i) \\ &= h(i) + V_{HF}(i) \end{aligned} \quad (2.9)$$

$(h(i)) = \text{core-Hamiltonian}$

and $V_{HF}(i) = \text{field potential}$

By incorporating basis functions, equation (2.8) can be transformed into a matrix form, commonly referred to as the Roothan-Hall equation:

$$\mathbb{F}\mathbf{C} = \mathbf{S}\mathbf{C}\mathbb{E} \quad (2.10)$$

where \mathbb{F} = Fock matrix, \mathbf{S} = overlap matrix, and \mathbf{C} = matrix of MO coefficient. In terms of orbital, the Hartree-Fock energy is

$$E_{HF} = \sum_a [a|h|a] + \frac{1}{2} \sum_a \sum_b [aa|bb] - [ab|ab] \quad (2.11)$$

In equation (2.11), the first term represents the one-electron integral, while the second term represents the two-electron integrals. These two-electron integrals consist of the Coulomb interaction term and the exchange interaction term, respectively.

Although the Hartree-Fock approximation provides a good starting point for many calculations, it has limitations and is not always accurate. More advanced methods, such as density functional theory, have been developed to address these limitations and provide a more accurate picture of molecular behavior. Nevertheless, the Hartree-Fock approximation remains a widely used and useful method for understanding the behavior of electrons in molecules.

2.1.4. Density functional theory

Density functional theory (DFT) [49-51] is a method used in quantum chemistry to calculate the electronic structure of molecules and solids. It is based not on the wavefunction but rather on the electron density. This allows for a more efficient and accurate calculation of the electronic structure of molecules and solids, as it considers

the interactions between electrons in a more sophisticated way than methods such as the Hartree-Fock approximation.

The key advantage of DFT is that it can accurately predict a wide range of properties of molecules and solids, such as their stability, reactivity, and spectra. It is widely used in materials science, chemistry, and physics. The principle of DFT is based on the Hohenberg-Kohn theorem and Kohn-Sham equation. The exchange-correlation functional in DFT is related to the accuracy of DFT.

The energy of DFT can be expressed in its most basic form as follows: can be written in its simplest form as:

$$E_{DFT} = T[\rho] + V_{ext}[\rho] + V_{ee}[\rho] \quad (2.12)$$

or in the line of the Kohn-Sham equation

$$E_{DFT} = T_s[\rho] + V_{ext}[\rho] + J[\rho] + E_{xc}[\rho] \quad (2.13)$$

In this context, the energy of DFT can be written in its simplest form, with the following components:

$T[\rho]$ represents the kinetic energy,

$T_s[\rho]$ represents the kinetic energy of the non-interacting system,

$V_{ee}[\rho]$ represents the electron-electron repulsion,

$J[\rho]$ represents the Coulomb interaction,

$V_{ext}[\rho]$ represents the external potential, and

$E_{xc}(\rho)$ represents the exchange-correlation functional.

The exchange-correlation functional of DFT can be classified into five generations, each representing a different level of sophistication and accuracy as shown in Figure 1 [52]. These generations are:

1. Local density approximation (LDA)

LDA functional depends only on the (local) density which can be treated as a uniform electron gas. The LDA expression for E_{xc} involves only the electron density (ρ).

Examples: S-VWN

2. Generalized gradient approximation (GGA)

GGA is an improvement functional over LDA to approach a non-uniform electron gas which makes the exchange-correlation energies dependent not only on the electron density but also on derivatives of the density, therefore GGA expressions for E_{xc} involve electron density (ρ) and gradient density ($\nabla\rho$).

Examples: PBE, BLYP and PW91

3. Meta-GGA (MGGA)

MGGA is an extension functional of GGA which allows the exchange and correlation functionals to depend on high-order derivatives of the electron density, with the Laplacian ($\nabla^2\rho$) being the second-order term. The MGGA expression for E_{xc} involves electron density (ρ), gradient density ($\nabla\rho$), and second gradient density ($\nabla^2\rho$).

Examples: M06-L, SCAN, TPSS, PKZB, and M11L.

4. Hybrid functionals or Hyper-GGA (HGGA)

HGGA mixes functionals between exchange and correlation energy components. This functional was first proposed by Axel Becke who combined LYP and PW91 to be B3LYP (Becke3-LYP) and B3PW91 (Becke3-PW91). HGGA adds the exact exchange (e_x^{exact}), hence it involves (ρ), ($\nabla\rho$), and (e_x^{exact}).

Examples: B3LYP, B3PW91, M06-2X, ω B97X-V and PBE0.

5. Double-Hybrid Functionals (DHDF)

DHDF is a functional which employed KS orbitals not only the occupied orbitals but also the virtual (unoccupied) orbitals. This functional was first proposed by Stefan Grimme with improving DFT energy results by using the MP2 second-order energy-correction formula and uses this functional to self-consistently solve for KS orbitals (both occupied and virtual).

Examples: B2PLYP, mPW2PLYP, PWPB95, B2GPPLYP, and DSD-PBEB95

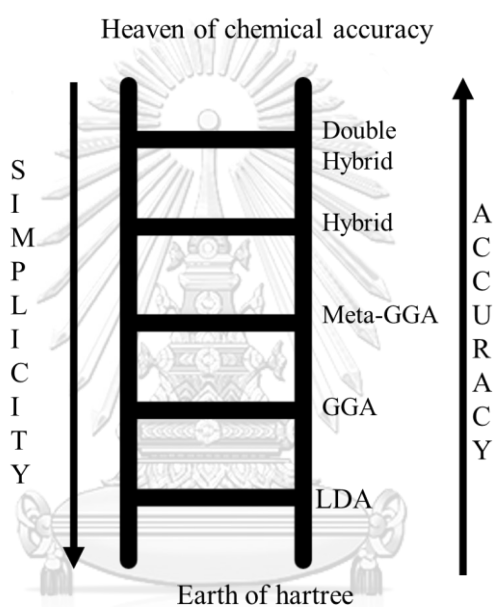


Figure 1. Jacob's ladder diagram of DFT hybrid functionals.

2.1.5. Basis set

Basis set [50] is a set of mathematical functions that are used to construct wavefunction according to the linear combination of atomic orbital-molecular orbital (LCAO-MO) approximation. It is very important as input data for the computational model in chemistry, physics, material science, and biology that is calculated by quantum calculation. The choice of basis set can affect the accuracy of quantum chemical calculations. There are two main types of basis sets: minimal and extended basis sets. These basis sets utilize different types of orbitals, including Slater-type orbitals (STOs), Gaussian-type orbitals (GTOs), as well as various expansions such as double-zeta, triple-zeta, quadruple-zeta, split-valence, diffuse, and polarized basis sets. These basis sets play a crucial role in approximating the wave functions and describing the electronic structure of molecules in quantum chemical calculations.

2.2 RECHARGEABLE LITHIUM-ION BATTERY

The fundamental rechargeable Li-ion battery of portable electronic technology was first introduced in 1991 with Sony Corporation's [53] that employed graphite host anode, LiCoO_2 cathode, and Li_xC_6 /non-aqueous liquid as electrolytes. The Li-ion battery achieved a high voltage (~ 3.7 V). The electrochemical process involves the Li-ion migration from cathode to anode and vice versa and released the electron [54] as shown in Figure. 2.

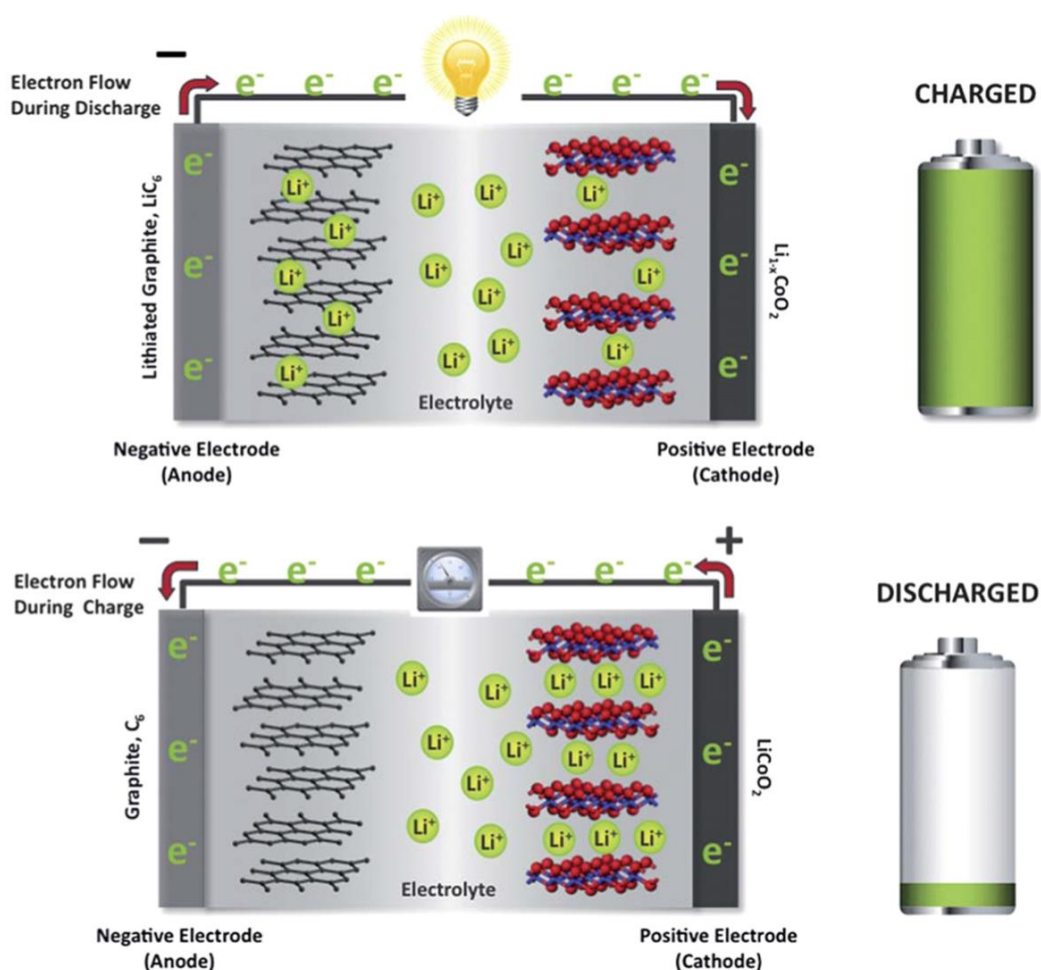


Figure 2. A schematic drawing illustrating the mechanism of rechargeable Li-ion batteries during the discharge and charge processes

In the discharge process of a lithium-ion battery, there is a migration of lithium ions from the lithiated graphite anode to the delithiated $\text{Li}_{1-x}\text{CoO}_2$ cathode. This migration is accompanied by oxidation and reduction reactions taking place at the respective electrodes. These reactions are described by equations (2.14-2.16). Conversely, during the charging process, the reverse mechanism occurs, with lithium ions migrating from the cathode back to the anode, and the corresponding oxidation and reduction reactions are reversed.

Positive electrode reaction (with charging being forward):



Negative electrode reaction (with charging being forward):



Total reaction:



CHAPTER III

DETAILS OF THE CALCULATION

3.1 LITHIUM ABSORPTION ON BULK SILICON

A bulk silicon structure was utilized, with determination based on the analysis of the X-ray diffraction (XRD) pattern in the BIOVIA Materials Studio [55] as shown in Figure 3. Two model sites, namely Tetrahedral (Td) and Hexagonal (Hex), were adopted for the lithium absorption sites, based on the study conducted by Wan et al. [23]. The DFT calculations were performed using the PBE0 hybrid functional [56] and the valence triple- zeta polarization (TZVP) basis set [57] within the CRYSTAL17 package [58].

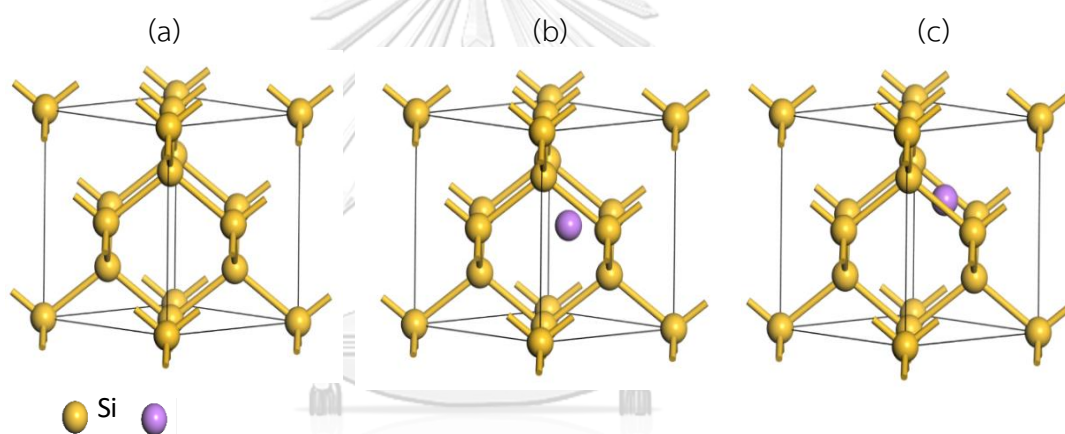


Figure 3. The structure of (a) bulk silicon with two absorption sites: (b) Tetrahedral and (c) Hexagonal.

3.2 LITHIUM ABSORPTION AND ADSORPTION ON SILICON QUANTUM DOTS

To facilitate a comparison with the bulk structures, ten different sizes of silicon quantum dots (SiQDs) were employed: $\text{Si}_{10}\text{H}_{16}$, $\text{Si}_{14}\text{H}_{20}$, $\text{Si}_{18}\text{H}_{24}$, $\text{Si}_{22}\text{H}_{28}$, $\text{Si}_{26}\text{H}_{30}$, $\text{Si}_{30}\text{H}_{34}$, $\text{Si}_{35}\text{H}_{36}$, $\text{Si}_{39}\text{H}_{40}$, $\text{Si}_{44}\text{H}_{42}$, and $\text{Si}_{48}\text{H}_{46}$ as a model for zero-dimensional (0D) silicon nanostructures. The sizes of these SiQDs were adopted from previous works by Xu et al. [59] and Li et al. [60], as illustrated in Figure 4. Two different lithium absorption sites: Tetrahedral (Td) and Hexagonal (Hex) and three different lithium adsorption sites:

hollow (H), bridge (B), and on-top (T) were considered. Illustrations structures were displayed in Figure 5. Also, apart from single Li atom adsorption double and triple adsorptions of Li atom were considered. All calculations were conducted using the density functional theory (DFT) method with the M06-2X hybrid functional [61] and the 6-31G+(d) basis set. The Gaussian16 software [62] was employed for these calculations. Following geometry optimization, we assigned the label "Td_{inner}" to the tetrahedral absorption site and "Td_{surface}" to the hollow adsorption site, aligning with the nomenclature used in the previous study by Gonzalez et al [44].

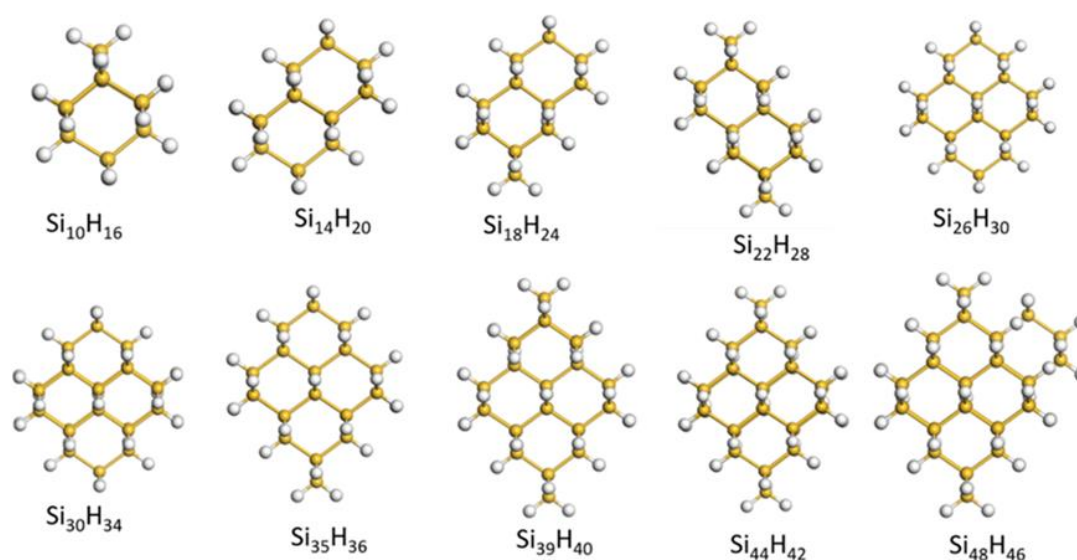


Figure 4. Ten models of silicon quantum dots (SiQDs)

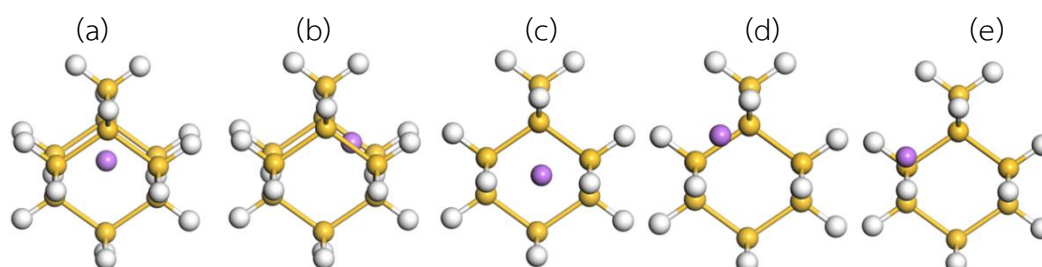


Figure 5. Two absorption sites, (a) Tetrahedral and (b) Hexagonal and three adsorption sites (c) hollow, (d) bridge and (e) on-top

3.3 LITHIUM ABSORPTION AND ADSORPTION ON SILICON NANOWIRES AND NANOPORES

Clusters of silicon nanowires with three different diameters (1 nm, 1.5 nm, and 2 nm) displayed in Figure 6 were investigated as models for one-dimensional (1D) nanostructures. The absorption sites (Td_{inner}) and adsorption sites ($Td_{surface}$) were evaluated using single, double, and triple lithium atoms. To assess the impact of porosity in the silicon nanostructure, we introduced a pore into the SiNWs model. In Figure 7, it can be observed that the Li atom appears to be surrounded by numerous silicon atoms, creating the impression of being covered by them (a). However, the absence of silicon atom coverage on the Li atom can be attributed to the porous nature of the silicon nanowire structure (b). Additionally, we conducted single and multiple lithium adsorption experiments at this stage. The binding energy, energy gap, and molecular volume were utilized as parameters to assess the stability of the structure, electronic conductivity, and the life cycle of both SiNWs and SiNPs anode batteries. All calculations were performed using the DFT method with the M06-2X hybrid functional and the 6-31G+(d) basis set level.

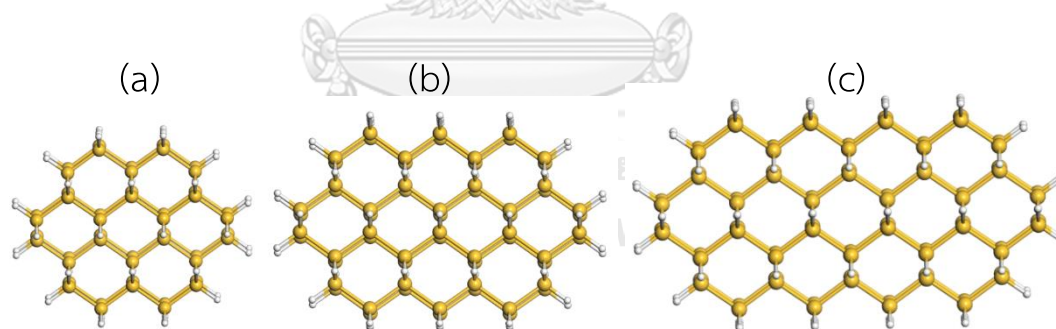


Figure 6. The surface of silicon nanowires with diameter of (a) 1 nm, (b) 1.5 nm and (c) 2 nm

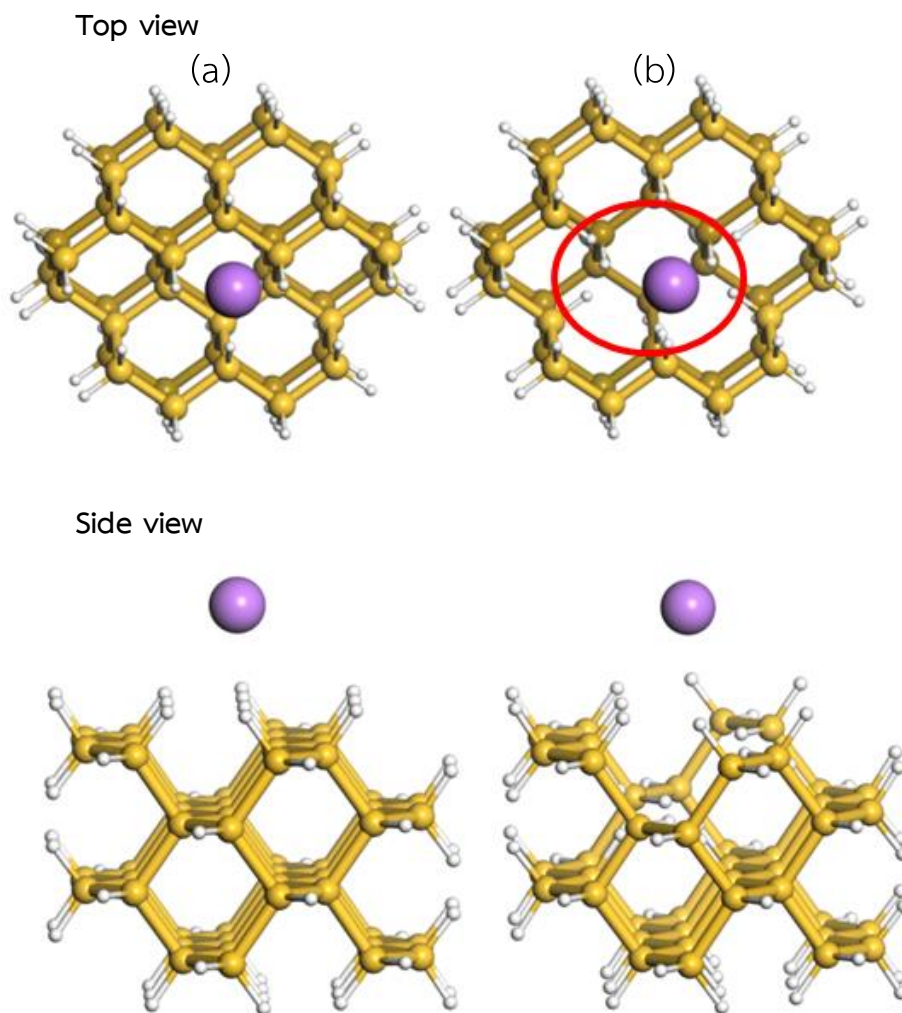


Figure 7. The structure of (a) silicon nanowires/SiNWs and (b) porous silicon nanowires/SiNPs with a diameter of 1 nm (top view) and length of 0.5 nm (side view).

3.4 Structural and electronic properties of lithium-silicon nanostructures (Li-SiNS)

To measure the interaction between lithium and silicon nanostructures, the binding energy per Li adsorption (E_{bind}) was calculated according to this equation:

$$E_{bind} = \frac{nE_{Li} + E_{SiNS} - E_{total}}{n_{Li}} \quad (3.1)$$

where E_{bind} is the binding energy between Li and SiNS, E_{Li} is the total energy of the Li atom, E_{SiNS} is the total energy of silicon nanostructures and E_{total} is the total energy of the Li-SiNS complex. According to this definition, a positive value of E_{bind} denotes a favorable adsorption process.

Then, we measure the percentage of SiNS molecular-volume change (ΔMV) to monitor the volume expansion after Li adsorption using this equation:

$$\Delta MV = \frac{[MV_{Li-SiNS} - MV_{SiNS}]}{MV_{SiNS}} \times 100 \quad (3.2)$$

where MV_{SiNS} and $MV_{Li-SiNS}$ are molecular volumes of the silicon nanostructure, before and after lithium adsorptions, respectively.

The energy gap (E_g) is defined using:

$$E_g = E_{LUMO} - E_{HOMO} \quad (3.3)$$

In this context, E_{LUMO} refers to the energy of the lowest unoccupied molecular orbital (LUMO), while E_{HOMO} represents the energy of the highest occupied molecular orbital (HOMO).

CHAPTER IV

RESULTS AND DISCUSSION

4.1 LITHIUM ABSORPTION ON BULK SILICON

4.1.1 Binding of Li to silicon bulk and volume expansion

The first model of silicon anodes with bulk silicon was examined using periodic calculations. As shown in Table 1, the results indicate that the binding energies of the absorption sites were measured to be 1.58 eV and 1.12 eV for the tetrahedral (Td) and hexagonal (Hex) configurations, respectively. This suggests that the tetrahedral structure is more thermodynamically stable compared to the hexagonal configuration, which aligns with previous findings [23, 44]. Additionally, we quantified the molecular volume changes in the bulk silicon, revealing values of 2.36% and 5.56% for the Td and Hex configurations, respectively. This observation suggests that lithium absorption on the hexagonal site has a greater impact on the volume expansion of the silicon anode material compared to the tetrahedral site. Therefore, the tetrahedral site can be recommended due to its favorable structural stability and lower volume expansion compared to the hexagonal site.

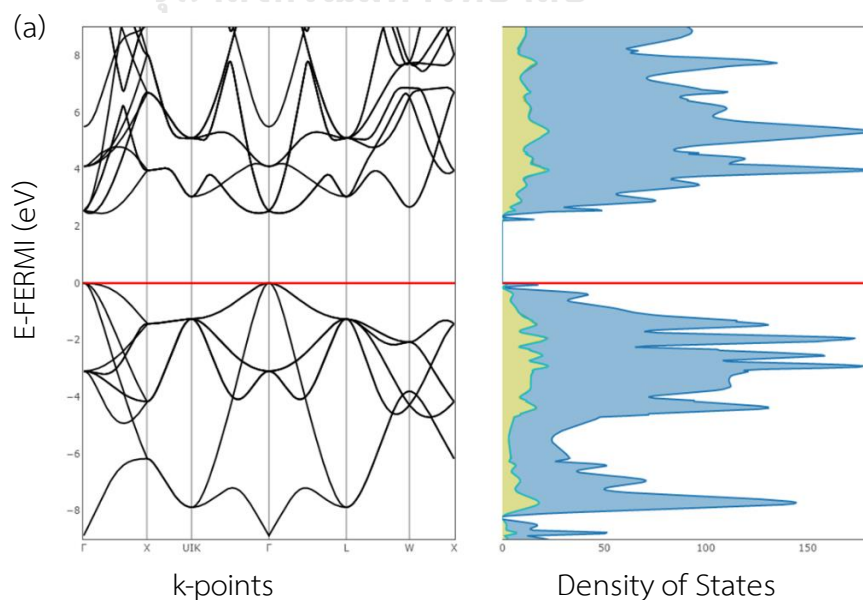
Table 1. Binding energy per Li adsorption (E_{bind}), the change of molecular volume (ΔMV), and the band gap energy (E_g) of Li-Si bulk structures.

Structure	E_{bind} (eV)	ΔMV (%)	E_g (eV)
Li-Td	1.58	2.36	2.00
Li-Hex	1.12	5.56	0.84

4.1.2 Effect of Li absorption on the band gap of silicon

The electronic properties of silicon nanostructures were investigated. The band gap energy of silicon as a semiconductor was determined to be 2.2 eV through calculations, aligning with previous research findings [23, 25]. Allowing lithium absorption, lithium is preferred to occupy the interstitial site, exhibiting characteristics of a shallow donor. This was observed in two distinct models: the tetrahedral (Td) and hexagonal (Hex) sites. For the Td configuration, the band structures exhibit minimal changes, with the band gap value remaining at 2.0 eV. However, the presence of interstitial Li causes a downward shift of the Fermi level towards the lower edge of the conduction band, resembling the behavior of n-type doping. This shift suggests that Li donates a portion of its 2s electron to Si. This observation is further supported by the density of states (DOS) spectra, which display the shifted Fermi level and an increased abundance of electrons in each orbital level.

In contrast, the hexagonal site exhibits a narrower band gap of 0.84 eV. Moreover, the Fermi level shift towards the edge of the conduction band is more pronounced compared to the Td configuration, as evident from Figure 8. This indicates that the choice of interstitial/absorption site has a significant impact on the alteration of the Fermi energy. Consequently, we can conclude that different absorption sites have a varying influence on the Fermi energy change.



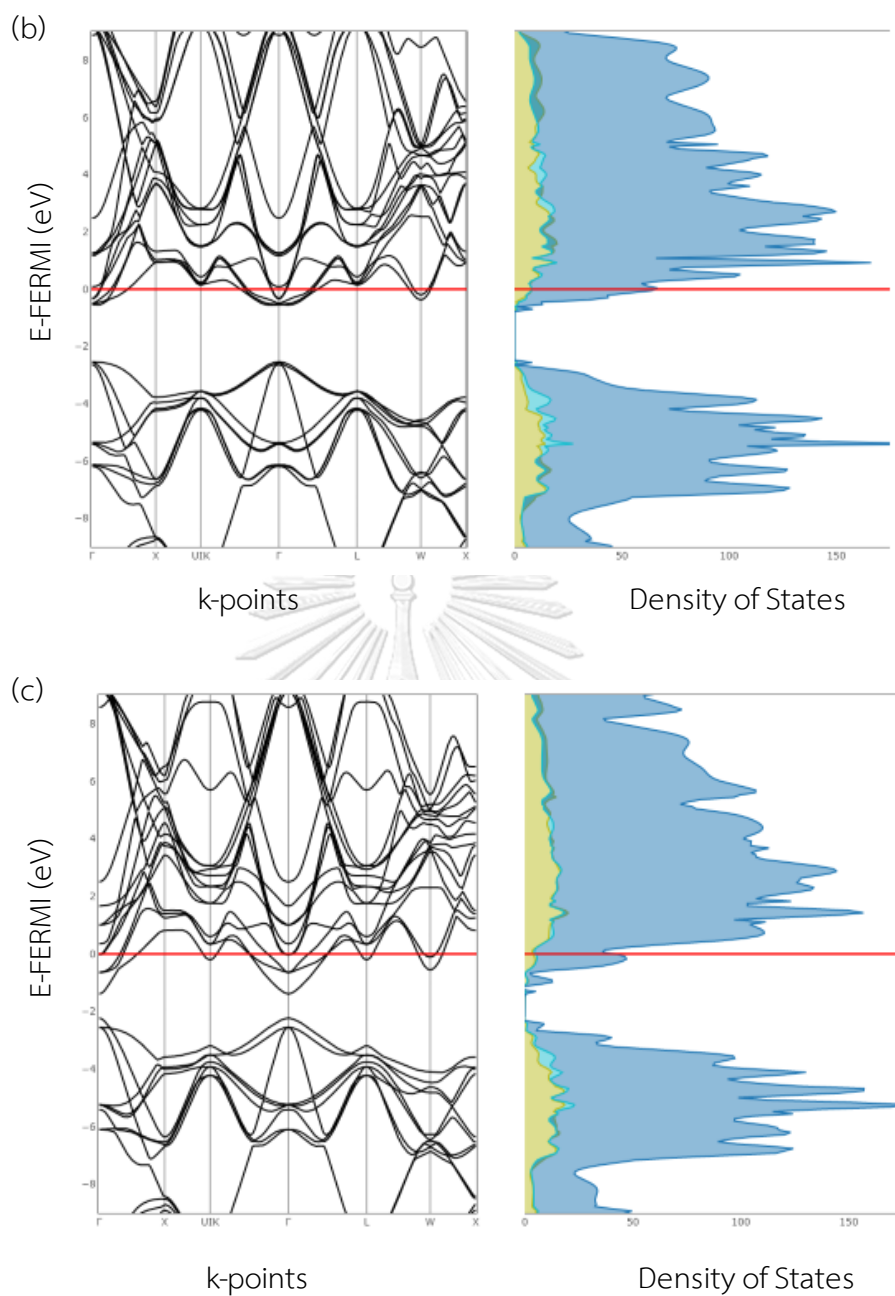


Figure 8. Band gap and DOS profile of (a) Bulk structures of silicon with two absorption sites: (b) Td and (c) Hex

4.2 LITHIUM ABSORPTION AND ADSORPTION ON SILICON QUANTUM DOTS

4.2.1 Binding of Li to SiQDs

Absorption and adsorption of lithium on silicon quantum dots (SiQDs) were investigated, and a total of 43 structures representing different configurations of Li interacting with the SiQDs were analyzed. These structures were categorized based on the specific absorption and adsorption sites, as summarized in Table 2. The binding energies for each complex were also reported. Specifically, the complexes consisted of 10 tetrahedral (Td), 9 hexagonal (Hex), 10 hollow (H), 7 bridge (B), and 7 on-top (T) structures. Upon comparing the adsorption at hollow, bridge, and on-top sites, we observed that the adsorption at the hollow sites exhibited stronger binding energies for the same SiQD. This finding is consistent with previous studies [14, 15] that have reported similar trends, indicating the preferential stronger binding of Li at the hollow sites. Therefore, our focus was primarily on the hollow site as an adsorption site, along with the Td and Hex configurations as absorption complexes. Consistent with the nomenclature employed in the previous study by Gonzalez et al. [44], we designated the tetrahedral absorption site as Td_{inner} and referred to the hollow adsorption site as $Td_{surface}$.

The binding energies of single Li absorption and adsorption in the hollow site of SiQDs range from -0.57 to +1.00 eV, as presented in Table 2 and Figure 9. These binding energies can be classified into three categories. "Strong" interactions, characterized by binding energies above 0.5 eV, indicate a favorable and stable binding. "Weak" interactions, with binding energies between 0.2 and 0.5 eV, suggest a relatively weaker but still present interaction. Conversely, binding energies with negative values represent an "unstable" binding, signifying a decrease in system stability after Li absorption, making it unlikely for Li to be absorbed in those sites. Figure 9 reveals that the absorption of Li on the Td_{inner} site exceeds 0.75 eV, while adsorption on the $Td_{surface}$ site remains below 0.5 eV but remains positive across all SiQDs. In contrast, Li absorption on the Hex site exhibits negative binding for the same SiQDs. Consequently, it can be inferred that the Td_{inner} site offers strong absorption, whereas $Td_{surface}$ and Hex provide weak adsorption and unstable absorption, respectively. Therefore, Td_{inner}

emerges as the most preferred absorption site for Li in all SiQDs. Additionally, it is noteworthy that the binding energy of Li to SiQDs varies with the absorption and adsorption positions, rather than the cluster size.

Table 2. The 43 structures of the absorption and adsorption complex of Li-SiQDs

SiQDs	Binding energy value (eV)				
	Td _{inner}	Hex	H (Td _{surface})	B	T
Si ₁₀ H ₁₆	0.95	H	0.22	T	0.11
Si ₁₄ H ₂₀	1.00	-0.57	0.22	0.13	0.10
Si ₁₈ H ₂₄ ,	0.81	-0.51	0.26	0.11	0.08
Si ₂₂ H ₂₈	0.83	-0.47	0.26	T	0.12
Si ₂₆ H ₃₀	0.81	-0.44	0.25	0.14	B
Si ₃₀ H ₃₄ ,	0.80	-0.40	0.26	0.17	0.20
Si ₃₅ H ₃₆	0.86	-0.41	0.28	0.23	B
Si ₃₉ H ₄₀	0.97	-0.42	0.23	0.15	0.18
Si ₄₄ H ₄₂	0.89	-0.33	0.30	0.09	B
Si ₄₈ H ₄₆	0.90	-0.35	0.22	H	0.17

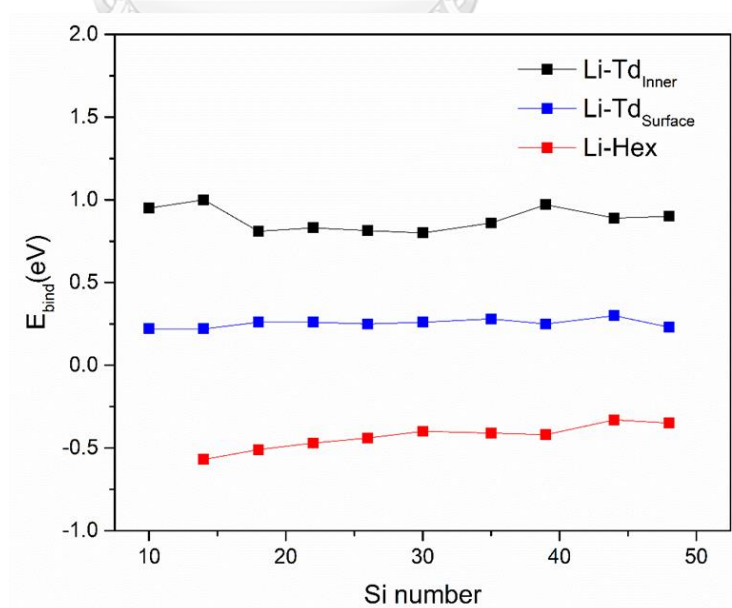


Figure 9. Binding energy of single Li for three sites: Td_{inner}, Td_{surface}, and Hex

In addition to single Li adsorptions, our study also investigated the multiple adsorptions of Li on SiQDs. This property provides insights into the charge density or capacity of SiQDs and tells how much charge can be stored in a battery. Specifically, we focused on double (2Li) and triple (3Li) adsorptions by adding second and third Li atoms to the single Li adsorption complexes and conducting subsequent geometry optimization. We only considered adsorptions in the Td_{surface} site since it was the only site obtained after geometry optimization. Binding energies per Li adsorption for double and triple adsorptions of Li were then compared to the corresponding single Li adsorptions.

Table 3. Binding energy (E_{bind}) of single and multiple Li adsorption on SiQDs

Si number	E_{bind} (eV)				
	Li- Td_{inner}	Li-Hex	Li- Td_{surface}		
			Li	2Li	3Li
Si ₁₀ H ₁₆	0.95	-	0.22	0.65	0.74
Si ₁₄ H ₂₀	1.00	-0.57	0.22	0.65	0.98
Si ₁₈ H ₂₄	0.81	-0.51	0.26	0.65	0.78
Si ₂₂ H ₂₈	0.83	-0.47	0.26	0.65	0.78
Si ₂₆ H ₃₀	0.81	-0.44	0.25	0.60	0.97
Si ₃₀ H ₃₄	0.80	-0.40	0.26	0.62	0.72
Si ₃₅ H ₃₆	0.86	-0.41	0.28	0.61	1.05
Si ₃₉ H ₄₀	0.97	-0.42	0.18	0.62	1.12
Si ₄₄ H ₄₂	0.89	-0.33	0.30	0.61	1.11
Si ₄₈ H ₄₆	0.90	-0.35	0.23	0.61	1.07

Table 3 provides the binding energies for double and triple Li adsorptions on different SiQDs. It is observed that the double Li adsorption exhibits binding energies around 0.60 eV, whereas the triple Li adsorption ranges from 0.72 to 1.12 eV. This indicates that the binding energy per Li adsorption increases as more Li atoms are adsorbed onto the SiQDs. Consequently, multiple Li adsorptions enhance the overall

binding energy and stability of the structures, suggesting a potential improvement in charge density and capacity for SiQDs in battery applications.

Among the SiQDs studied, $\text{Si}_{39}\text{H}_{40}$, $\text{Si}_{44}\text{H}_{42}$, and $\text{Si}_{48}\text{H}_{46}$ exhibited the highest E_{bind} for triple Li adsorption. This finding contrasts with the results reported by Pattarapongdilok and Parasuk [12], who studied multiple Li adsorptions in Graphene Quantum Dots (GQDs) and found that the binding of Li atoms to GQDs weakened with the addition of more Li atoms. Additionally, the study by Hu and Zhou [22] revealed that the average binding energy for multiple Li adsorptions on GQDs was smaller than that of single Li atom adsorption.

Our study suggests that SiQDs, as an anode material, can provide a higher charge density compared to graphene-based anodes. While the Td_{inner} site is the most preferred for single Li adsorption, the $\text{Td}_{\text{surface}}$ site becomes more advantageous in the case of multiple Li adsorptions. This preference for the $\text{Td}_{\text{surface}}$ site in multiple adsorptions could be attributed to the limited space within the SiQDs, as our largest Si cluster consisted of only 48 Si atoms. In such cases, Li tends to adsorb on the surface (outside) rather than being accommodated within the cluster. It is worth considering that larger SiQDs may be capable of accommodating more Li atoms inside the cluster, thereby favoring the Td_{inner} site.

4.2.2 Effect of Li absorption and adsorption on the volume expansion

To investigate the potential volume expansion resulting from Li absorption and adsorption on SiQD anode materials, we monitored the molecular volume of the SiQDs before and after lithiation. Volume expansion is a critical factor that can impact the overall performance and cycle life of batteries, particularly in the case of silicon anodes. By comparing the molecular volumes of SiQDs before and after lithiation, we can assess whether there is a significant change in volume. This analysis provides valuable insights into the expansion behavior of SiQDs upon Li interaction and helps us understand the potential challenges associated with volume expansion in silicon anodes for lithium-ion batteries. The molecular volume of a molecule refers to the space it occupies, which is non-penetrable to other molecules under normal conditions. The van der Waals volume is commonly employed as an approximation, determined by considering the outer surface of the interpenetrating spheres surrounding the molecule. This approach, based on the concept of intermolecular forces, allows for an estimation of the molecular volume, and is commonly used in scientific studies [63, 64]. By utilizing this method, we can assess the changes in molecular volume of SiQDs before and after lithiation, providing insights into the volume expansion effects associated with Li absorption and adsorption on the SiQD anode material [63, 64]. Molecular volumes for ten bare SiQDs ($\text{Si}_{10}\text{H}_{16}$, $\text{Si}_{14}\text{H}_{20}$, $\text{Si}_{18}\text{H}_{24}$, $\text{Si}_{22}\text{H}_{28}$, $\text{Si}_{26}\text{H}_{30}$, $\text{Si}_{30}\text{H}_{34}$, $\text{Si}_{35}\text{H}_{36}$, $\text{Si}_{39}\text{H}_{40}$, $\text{Si}_{44}\text{H}_{42}$, and $\text{Si}_{48}\text{H}_{46}$) and those with Li absorption and adsorption at three sites, i.e., Td_{inner} , Hex, and $\text{Td}_{\text{surface}}$ were calculated. The percentage change in molecular volume (ΔMV) was used to justify the volume change of SiQDs after lithiation.

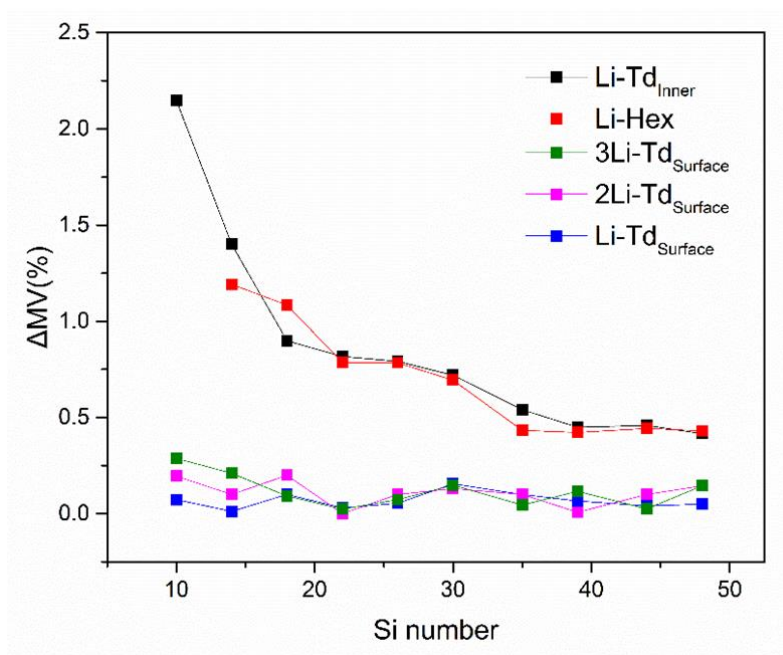


Figure 10. The percentage change in molecular volume of SiQDs after Li adsorption

In Figure 10, the percentage change in molecular volume after lithiation of various SiQDs is illustrated. For single Li absorption and adsorption, the percentage change in molecular volume of SiQDs ranged from 0.42% to 2.15% for absorption in the Td_{inner} and Hex sites. In contrast, much smaller changes were observed for adsorption in the Td_{surface} site, with percentage volume changes ranging from 0% to 0.29%. Notably, the percentage change in volume did not vary with the number of Li adsorptions in the Td_{surface} site.

For Li absorptions in the Td_{inner} and Hex sites, the percentage change in volume exhibited variation based on the size of the SiQD. Specifically, larger volume changes were observed for smaller SiQDs. For instance, Si₁₀H₁₆ showed a percentage volume change of 2.15%, while Si₄₈H₄₆ exhibited a change of 0.42%. Therefore, lithiation in the Td_{surface} site resulted in less volume change compared to the Td_{inner} and Hex sites. These findings shed light on the extent of volume expansion experienced by SiQDs upon lithiation, with implications for the performance and stability of Si-based anode materials in lithium-ion batteries.

This observation can be explained by considering the location of the Td_{inner} and Hex sites inside the SiQD cluster. When Li atoms are absorbed in these sites, they require space within the cluster, resulting in expansion of the molecular framework. In larger SiQD clusters, there is more available space inside, which allows for accommodating Li atoms without significant volume expansion. This explains the smaller volume expansion observed for absorption in larger clusters. On the other hand, the Td_{surface} site, where adsorption takes place outside the SiQD cluster, has a limited effect on the molecular framework. As a result, only a very small volume expansion was observed, and this expansion did not depend on the cluster size or the number of Li adsorptions. Based on these findings, we recommend using larger-sized SiQDs as anode materials for Li-ion batteries. This is because the integrity of their structures can be maintained upon Li deposition, with minimal volume changes. Using larger-sized SiQDs ensures that the batteries can effectively accommodate Li without significant expansion, enhancing the stability and overall performance of the anode material.

4.2.3 Effect of Li absorption and adsorption on the energy gap

The electrical conductivity of silicon anode is considered a drawback when compared to carbon-based anodes. This is primarily due to the intrinsic nature of silicon crystal, which is a semiconductor with a band gap of approximately 1.2 eV [65]. In contrast, graphite, which is commonly used in carbon-based anodes, exhibits conductivity as it is a conductor. In the case of non-periodic systems, such as SiQDs, the concept of a band gap is not directly applicable. Instead, the energy difference between the highest occupied molecular orbital (E_{HOMO}) and the lowest unoccupied molecular orbital (E_{LUMO}) is employed to estimate the energy gap (E_g). This energy gap helps to address the conductivity characteristics of these materials, providing insights into their electrical properties. By considering the energy gap (E_g) as an indicator of conductivity, it becomes evident that silicon anodes face challenges due to their semi-conducting nature compared to the conductive nature of carbon-based anodes. Understanding these differences in electrical conductivity is crucial in assessing and optimizing the performance of Si-based anodes in lithium-ion battery systems.

Table 4. Energy gaps (E_g) of various sizes of SiQDs and nLi-SiQDs

SiQDs	HOMO-LUMO Energy gap (eV)					
	without Li	Td_{inner}	Hex	Td_{surface}		
				Li	2Li	3Li
$Si_{10}H_{16}$	8.09	4.12	-	3.29	3.34	2.63
$Si_{14}H_{20}$	7.43	3.96	3.05	3.11	3.18	2.76
$Si_{18}H_{24}$	7.06	3.63	2.84	3.06	3.20	2.47
$Si_{22}H_{28}$	6.90	3.52	2.73	2.98	3.16	2.40
$Si_{26}H_{30}$	6.73	3.36	2.62	2.73	2.83	2.62
$Si_{30}H_{34}$	6.69	3.30	2.54	2.67	2.80	2.16
$Si_{35}H_{36}$	6.55	3.17	2.47	2.55	2.68	3.48
$Si_{39}H_{40}$	6.25	3.32	2.40	2.40	2.64	3.47
$Si_{44}H_{42}$	6.08	3.13	2.37	2.39	2.74	2.94
$Si_{48}H_{46}$	5.95	3.11	2.38	2.33	2.49	2.81

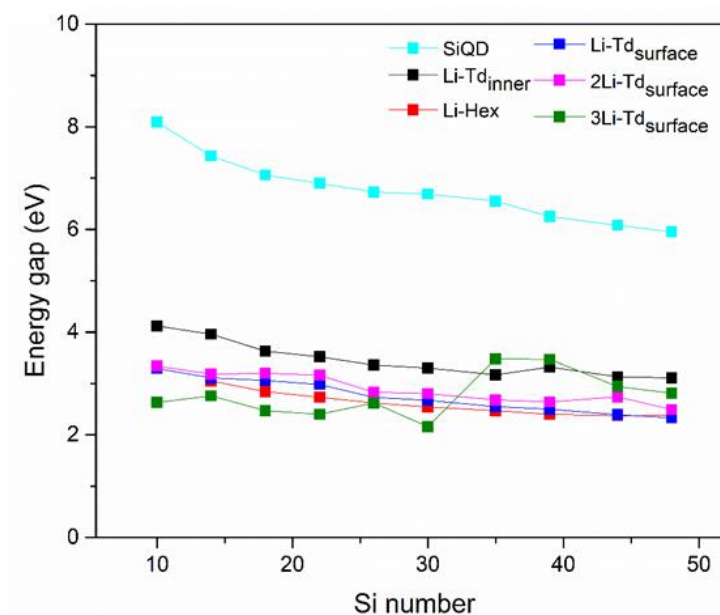


Figure 11. Energy gaps of various sizes of un-adsorbed and nLi-adsorbed SiQDs

Table 4 and Figure 11 provide information on the energy gaps (E_g) of bare SiQDs, as well as SiQDs with adsorbed and adsorbed Li. The energy gaps of bare SiQDs range from 5.95 eV ($\text{Si}_{48}\text{H}_{46}$) to 8.09 eV ($\text{Si}_{10}\text{H}_{16}$), and it is evident that the E_g varies with the cluster size, with larger SiQDs exhibiting smaller E_g values. Notably, there is a significant difference of 2.34 eV in E_g between the smallest and largest values, highlighting the influence of cluster size on the energy gap. After the absorption and adsorption of Li, a substantial reduction in the energy gap is observed, indicating increased conductivity of the SiQDs. Figure 11 demonstrates this reduction in E_g . For single Li absorption, the energy gaps range from 2.33 eV to 4.12 eV, resulting in a reduction of approximately 4 eV compared to the bare SiQDs. These findings indicate that the lithiation process leads to a significant decrease in the energy gap of SiQDs, making them more conductive. This reduction in energy gap is crucial for improving the electrical conductivity of Si-based anodes, addressing one of the limitations of Si as an anode material compared to carbon-based alternatives. Furthermore, it should be noted that

the energy gap (E_g) is not only influenced by the cluster size but also by the specific absorption and adsorption sites, as well as the number of Li atoms adsorbed.

However, the differentiation of the energy gap based on these factors is not as pronounced. When comparing different absorption and adsorption sites, SiQDs with Li absorption on Td_{inner} exhibit the largest E_g , followed by adsorption in $Td_{surface}$ and absorption in Hex sites. For the adsorption in $Td_{surface}$, the presence of double Li adsorption increases the E_g of SiQDs by values ranging from 0.05 to 0.35 eV, depending on the cluster size. On the other hand, the triple Li adsorption results in a reduction of E_g for small SiQDs ($n=10-30$) with values ranging from -0.66 to -0.11 eV, while medium to large SiQDs ($n=34-46$) experience an increment in E_g ranging from 0.48 to 1.03 eV. These observations indicate that both single and multiple Li absorptions and adsorptions have an impact on the energy gap.

This phenomenon demonstrates the ability of SiQDs as semiconductor materials to accept and release electrons, which aligns with previous studies [14, 15]. The variations in the energy gap highlight the influence of Li absorption and adsorption on the electronic properties of SiQDs, further emphasizing their potential as functional materials for energy storage applications.

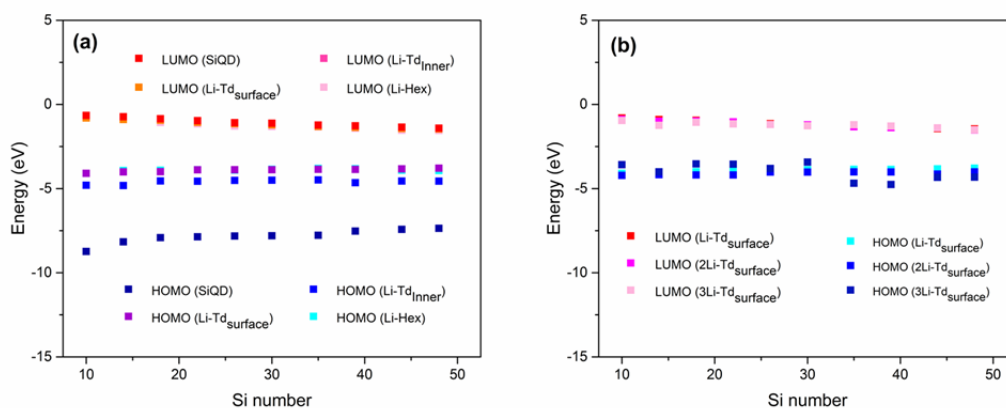


Figure 12. HOMO, LUMO energies (eV) of SiQDs, (a) single and (b) multiple Li adsorbed on SiQDs (Li-SiQDs and nLi-SiQDs)

We present the energies of the highest occupied molecular orbital (HOMO) and the lowest unoccupied molecular orbital (LUMO) for bare SiQDs, as well as Li-absorbed and Li-adsorbed SiQDs in various sites in Figure 12a. The changes in HOMO and LUMO energies provide insights into the electronic structure of SiQDs upon Li absorption and adsorption. The figure 12b specifically focuses on the effect of single, double, and triple Li adsorptions on the HOMO and LUMO energies of SiQDs. This analysis allows us to observe the impact of multiple Li adsorptions on the electronic properties of SiQDs. By monitoring the changes in HOMO and LUMO energies, we gain a deeper understanding of how Li absorption and adsorption influence the electronic structure of SiQDs, providing valuable information for the design and optimization of Si-based anode materials in lithium-ion batteries.

We observe that the LUMO energies of SiQDs remain relatively unchanged upon Li absorption and adsorption. However, the HOMO energies of bare SiQDs show a significant increase after lithiation, resulting in a decrease in the energy gap. This reduction in the energy gap is primarily driven by the increment of HOMO energies associated with Li absorption and adsorption. The HOMO energies for bare SiQDs are within the range of -10 to -7.5 eV, whereas for Li-absorbed and Li-adsorbed SiQDs, they are around -5 eV. Notably, the HOMO energy of the Li atom itself is measured at -4.16 eV. Hence, the increase in HOMO energies can be attributed to the energy level of the Li atom upon absorption.

Interestingly, the increment in HOMO energies is predominantly influenced by the specific absorption and adsorption sites (Td_{surface} and Hex), rather than the cluster size. Among the sites, Td_{surface} and Hex exhibit the most significant changes in HOMO energies, while Td_{inner} shows a comparatively smaller effect. Moreover, the adsorption of second and third Li atoms does not significantly alter the HOMO energy of SiQDs, indicating that their impact on the electronic structure is limited in this context.

These findings highlight the role of Li absorption and adsorption in modifying the electronic properties of SiQDs, specifically through the modulation of HOMO

energies. Understanding these changes is crucial for enhancing the performance and design of Si-based anode materials in lithium-ion batteries. Hence, the presence of multiple Li adsorptions is unlikely to have a significant impact on the energy gap of Li-adsorbed SiQDs. Consequently, based on our research findings, we can deduce that large-sized SiQDs exhibit favorable characteristics as anode materials for Li-ion batteries. This is primarily attributed to their notable capacity for Li adsorption, minimal volume expansion, and satisfactory conductivity.



4.3 LITHIUM ABSORPTION AND ADSORPTION ON SILICON NANOWIRE AND NANOPORE

4.3.1 Binding of Li to SiNWs with diameters of 1 nm, 1.5 nm, and 2 nm

We observed that adsorptions in Td_{inner} and $Td_{surface}$ sites give the most stable binding from section 4.2. With this information, we proceeded to investigate the adsorption on both sites for silicon nanowires (SiNWs). In Table 5 and Figure 9, it is evident that the binding energies of $Td_{surface}$ are consistently larger than those of Td_{inner} for all SiNW models with 1 nm, 1.5 nm, and 2 nm diameters. The results also suggest that the diameter of the SiNWs has minimal influence on the binding energy. The binding energy depends more on the adsorption site and type of materials (SiNWs or SiNPs). The Li binding in SiNWs at $Td_{surface}$ (1.28 eV) is stronger than that at Td_{inner} (0.40 – 0.52 eV) and SiNPs (0.68 – 0.73 eV). However, the binding is weaker than in bulk (1.58 eV) but larger than SiQDs (~1 eV).

Table 5. Binding energy (E_{bind}) and energy gap (E_g) of Li absorption and adsorption on SiNWs and SiNPs

Structures	E_{bind} (eV)	E_g (eV)
SiNWs-1nm	-	5.92
Li- Td_{inner} -SiNWs-1nm	0.52	2.59
Li- $Td_{surface}$ -SiNWs-1nm	1.28	3.10
Li- $Td_{surface}$ -SiNPs-1nm	0.73	2.29
SiNWs-1.5nm	-	5.44
Li- Td_{inner} -SiNWs-1.5nm	0.42	2.29
Li- $Td_{surface}$ -SiNWs-1.5nm	1.28	2.91
Li- $Td_{surface}$ -SiNPs-1.5nm	0.68	2.62
SiNWs-2nm	-	5.14
Li- Td_{inner} -SiNWs-2nm	0.40	2.16
Li- $Td_{surface}$ -SiNWs-2nm	1.28	2.78
Li- $Td_{surface}$ -SiNPs-2nm	0.68	2.39

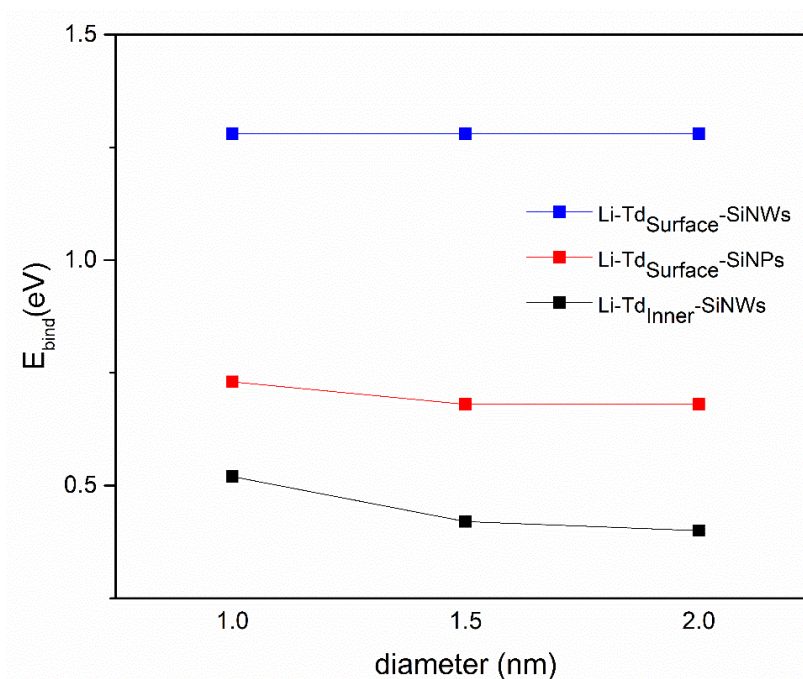


Figure 13. Binding energy of Li-SiNWs and Li-SiNPs

4.3.2 Effect of Li absorption, adsorption, and porosity on the energy gap

Subsequently, our investigation focused on examining the impact of Li absorption and adsorption on the electronic conductivity of SiNWs. We observed a significant decrease in the E_g of SiNWs after lithiation, indicating a substantial enhancement in their conductivity. In contrast to Li-Td_{inner}-SiNWs, Li-Td_{surface}-SiNWs exhibit a higher energy gap, suggesting lower conductivity. To enhance the conductivity of Td_{surface} structures, one potential solution could be the creation of surface pores on SiNWs. By introducing porosity, the conductivity of Li-Td_{surface}-SiNWs is effectively increased. Based on our calculations, the results indicate that SiNPs have a lower energy gap (2.29 eV) compared to SiNWs (3.10 eV). This observation suggests that the introduction of porosity in the material has a positive impact on enhancing conductivity. The porous structure appears to contribute to the increased conductivity of silicon nanowires.

Furthermore, we investigated the multiple adsorptions of Li on SiNWs. As demonstrated in Table 6, the binding energy of multiple adsorptions was found to be

lower than that of single adsorptions. Specifically, the binding energy of SiNWs decreases upon adsorption of the second Li atom, but it experiences a slight increase after the third Li atom is adsorbed. The highest binding energies recorded were 1.28 eV for the first Li atom, and 1.21 eV for both the second and third Li atoms. However, it is worth noting that porosity tends to increase the binding energy of $\text{Li}_2\text{-Td}_{\text{surface}}\text{-SiNWs-1nm}$ (0.67 to 0.79 eV), $\text{Li}_3\text{-Td}_{\text{surface}}\text{-SiNWs-1nm}$ (0.72 to 0.91 eV), $\text{Li}_2\text{-Td}_{\text{surface}}\text{-SiNWs-1.5nm}$ (0.68 to 0.74 eV) and $\text{Li}_3\text{-Td}_{\text{surface}}\text{-SiNWs-1.5nm}$ (0.72 to 0.91 eV). Conversely, it decreases the binding energy of $\text{Li}_2\text{-Td}_{\text{surface}}\text{-SiNWs-2nm}$ (1.21 to 0.82 eV), and $\text{Li}_3\text{-Td}_{\text{surface}}\text{-SiNWs-2nm}$ (1.21 to 0.94 eV).

Table 6. Binding energy (E_{bind}) and energy gap (E_g) of multiple Li adsorptions on SiNWs and SiNPs

Structures	E_{bind} (eV)	E_g (eV)
$\text{Li}_2\text{-Td}_{\text{surface}}\text{-SiNWs-1nm}$	0.67	2.49
$\text{Li}_2\text{-Td}_{\text{surface}}\text{-SiNPs-1nm}$	0.79	2.59
$\text{Li}_3\text{-Td}_{\text{surface}}\text{-SiNWs-1nm}$	0.72	1.87
$\text{Li}_3\text{-Td}_{\text{surface}}\text{-SiNPs-1nm}$	0.91	1.99
$\text{Li}_2\text{-Td}_{\text{surface}}\text{-SiNWs-1.5nm}$	0.68	2.26
$\text{Li}_2\text{-Td}_{\text{surface}}\text{-SiNPs-1.5nm}$	0.74	2.74
$\text{Li}_3\text{-Td}_{\text{surface}}\text{-SiNWs-1.5nm}$	0.72	1.72
$\text{Li}_3\text{-Td}_{\text{surface}}\text{-SiNPs-1.5nm}$	0.91	1.87
$\text{Li}_2\text{-Td}_{\text{surface}}\text{-SiNWs-2nm}$	1.21	2.91
$\text{Li}_2\text{-Td}_{\text{surface}}\text{-SiNPs-2nm}$	0.82	2.54
$\text{Li}_3\text{-Td}_{\text{surface}}\text{-SiNWs-2nm}$	1.21	2.91
$\text{Li}_3\text{-Td}_{\text{surface}}\text{-SiNPs-2nm}$	0.94	1.97

The introduction of the second and third Li atoms in SiNWs has a noticeable impact on reducing the energy gap and enhancing their electronic conductivity. For instance, in SiNWs with a diameter of 1 nm, the energy gap values are as follows: 3.10 eV for the first Li atom, 2.49 eV for the second Li atom, and 1.87 eV for the third Li atom. Furthermore, the influence of porosity on the electronic conductivity in the case of multiple adsorptions is not significant. The presence of porosity tends to slightly increase the energy gap: from 2.49 to 2.59 eV for $\text{Li}_2\text{-Td}_{\text{surface}}\text{-SiNWs-1nm}$, from 1.87 to 1.99 eV for $\text{Li}_3\text{-Td}_{\text{surface}}\text{-SiNWs-1nm}$, from 2.26 to 2.74 eV for $\text{Li}_2\text{-Td}_{\text{surface}}\text{-SiNWs-1.5nm}$ and from 1.72 to 1.87 eV for $\text{Li}_3\text{-Td}_{\text{surface}}\text{-SiNWs-1.5nm}$. However, it does have an impact on decreasing the energy gap: from 2.91 to 2.54 eV for $\text{Li}_2\text{-Td}_{\text{surface}}\text{-SiNWs-2nm}$ and from 2.91 to 1.97 eV for $\text{Li}_3\text{-Td}_{\text{surface}}\text{-SiNWs-2nm}$.

4.3.3 Effect of Li absorption and adsorption on the volume expansion

In our latest investigation, we closely monitored the changes in molecular volume of both SiNWs and SiNPs, following the methodology outlined in our previous report. The obtained results, as presented in Fig.4.7., reveal the following trends: $\Delta\text{MV}(\%)$ of $\text{Td}_{\text{inner}} > \text{Td}_{\text{surface}}\text{-SiNWs} > \text{Td}_{\text{surface}}\text{-SiNPs}$. This suggests that the $\text{Td}_{\text{surface}}$ sites exhibit less pronounced effects during lithiation compared to the Td_{inner} . The length of SiNWs also influences $\Delta\text{MV}(\%)$, since this value is further reduced as the length of SiNWs is extended. Moreover, it is observed that the second and third Li adsorptions lead to a reduction in $\Delta\text{MV}(\%)$, indicating that the molecular volume changes less as more Li is added. Compared to SiNPs, all SiNPs have small values of $\Delta\text{MV}(\%)$. Thus, introducing porosity in the structure causes the volume to change less. As a result, it is possible to achieve minimal volume changes upon lithiation by increasing the size of silicon nanostructures and introducing pores. These modifications help maintaining the structural integrity and stability of the silicon nanostructures during the lithiation process.

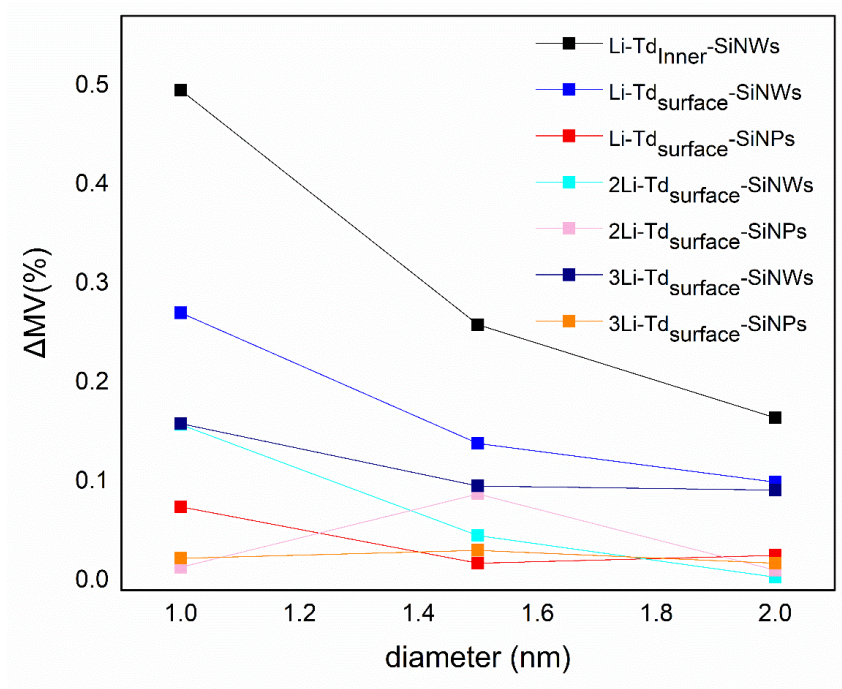


Figure 14. The percentage change in molecular volume of SiNWs and SiNPs after Li adsorption

CHAPTER V

CONCLUSION

We investigated the absorption and adsorption of lithium in silicon nanostructures, including silicon quantum dots (SiQDs), silicon nanowires (SiNWs), and silicon nanopores (SiNPs), while analyzing their structural and electronic properties in comparison to bulk silicon. Our findings reveal that the binding behavior between lithium and silicon nanostructures is strongly influenced by specific absorption and adsorption sites. Notably, we observed a strong binding on the Td_{inner} site for absorption and the $Td_{surface}$ site for adsorption.

In the case of SiQDs, we found a stronger binding on the Td_{inner} site with binding energies ranging from 0.80 to 1.00 eV, while adsorption on the $Td_{surface}$ site resulted in weaker binding energies between 0.18 and 0.30 eV. Interestingly, the binding of Li in the Hex site was consistently negative (unstable) for all SiQDs. Therefore, the Td_{inner} site emerges as the preferred site for SiQDs. Furthermore, we observed that the binding energy increases with the addition of more Li atoms to SiQDs, indicating their potential for accommodating a higher number of Li atoms per structure and enabling high-capacity anodes.

In SiNWs models with diameters of 1 nm, 1.5 nm, and 2 nm, we observed that the binding energies of $Td_{surface}$ consistently exceeded those of Td_{inner} . The diameter of the SiNWs structure showed minimal influence on the binding energy values. Interestingly, unlike SiQDs, multiple adsorptions in SiNWs resulted in lower binding energies compared to single adsorption. Additionally, our investigation revealed that porosity (SiNPs) did not significantly affect the binding energies in SiNWs structures.

To address the life cycle challenges of silicon anodes, we evaluated the change in molecular volume of various SiQDs after lithiation. Our results showed that the volume change did not vary with the number of Li adsorptions but depended on the site and cluster size. Larger SiQDs exhibited smaller volume changes, indicating that

they are less susceptible to volume expansion during lithiation. Furthermore, SiNWs and SiNPs showed minimal volume changes, with values below 0.5%. Larger diameters of SiNWs and SiNPs were associated with smaller volume changes. Multiple adsorptions further mitigated volume expansion. Hence, larger silicon nanostructures are recommended to avoid volume expansion during lithiation.

We also investigated the impact of lithiation on the electronic properties of silicon anode materials. Consistently, our results demonstrated that the presence of lithium decreased the resistivity of various silicon structures, including bulk silicon, SiQDs, SiNWs, and SiNPs, indicating increased conductivity. Moreover, the presence of pores in SiNWs led to a decrease in the energy gap, enhancing conductivity. Consequently, SiQDs, SiNWs, and SiNPs exhibit favorable characteristics as anode materials for Li-ion batteries, including high capacity, minimal volume expansion, and improved conductivity.

REFERENCES



จุฬาลงกรณ์มหาวิทยาลัย
CHULALONGKORN UNIVERSITY

- [1] Chen, W., Liang, J., Yang, Z., and Li, G. A review of lithium-ion battery for electric vehicle applications and beyond. Energy Procedia 158 (2019): 4363-4368.
- [2] Kim, T., Song, W., Son, D.-Y., Ono, L.K., and Qi, Y. Lithium-ion batteries: outlook on present, future, and hybridized technologies. Journal of materials chemistry A 7(7) (2019): 2942-2964.
- [3] Nitta, N., Wu, F., Lee, J.T., and Yushin, G. Li-ion battery materials: present and future. Materials today 18(5) (2015): 252-264.
- [4] Romare, M. and Dahllöf, L. The life cycle energy consumption and greenhouse gas emissions from lithium-ion batteries. 2017, IVL Svenska Miljöinstitutet.
- [5] Liang, Y., et al. Life cycle assessment of lithium-ion batteries for greenhouse gas emissions. Resources, conservation and recycling 117 (2017): 285-293.
- [6] Xu, C., Steubing, B., Hu, M., Harpprecht, C., van der Meide, M., and Tukker, A. Future greenhouse gas emissions of automotive lithium-ion battery cell production. Resources, Conservation and Recycling 187 (2022): 106606.
- [7] Chen, X., Shen, W., Vo, T.T., Cao, Z., and Kapoor, A. An overview of lithium-ion batteries for electric vehicles. in, pp. 230-235: IEEE.
- [8] Chen, S., Dai, F., and Cai, M. Opportunities and challenges of high-energy lithium metal batteries for electric vehicle applications. ACS energy letters 5(10) (2020): 3140-3151.
- [9] Franco Gonzalez, A., Yang, N.-H., and Liu, R.-S. Silicon anode design for lithium-ion batteries: progress and perspectives. The Journal of Physical Chemistry C 121(50) (2017): 27775-27787.
- [10] Jin, Y., Zhu, B., Lu, Z., Liu, N., and Zhu, J. Challenges and recent progress in the development of Si anodes for lithium-ion battery. Advanced Energy Materials 7(23) (2017): 1700715.
- [11] Sun, L., Liu, Y., Shao, R., Wu, J., Jiang, R., and Jin, Z. Recent progress and future perspective on practical silicon anode-based lithium ion batteries. Energy Storage Materials (2022).
- [12] Wu, H. and Cui, Y. Designing nanostructured Si anodes for high energy lithium ion batteries. Nano today 7(5) (2012): 414-429.

- [13] Xu, Z.-L., Liu, X., Luo, Y., Zhou, L., and Kim, J.-K. Nanosilicon anodes for high performance rechargeable batteries. Progress in Materials Science 90 (2017): 1-44.
- [14] Chan, C.K., et al. High-performance lithium battery anodes using silicon nanowires. Nature nanotechnology 3(1) (2008): 31-35.
- [15] Zhao, X. and Lehto, V.-P. Challenges and prospects of nanosized silicon anodes in lithium-ion batteries. Nanotechnology 32(4) (2020): 042002.
- [16] Zhang, C., et al. Challenges and recent progress on silicon-based anode materials for next-generation lithium-ion batteries. Small Structures 2(6) (2021): 2100009.
- [17] Ko, M., Chae, S., and Cho, J. Challenges in accommodating volume change of Si anodes for Li-ion batteries. ChemElectroChem 2(11) (2015): 1645-1651.
- [18] Entwistle, J., Rennie, A., and Patwardhan, S. A review of magnesiothermic reduction of silica to porous silicon for lithium-ion battery applications and beyond. Journal of Materials Chemistry A 6(38) (2018): 18344-18356.
- [19] Ge, M., Fang, X., Rong, J., and Zhou, C. Review of porous silicon preparation and its application for lithium-ion battery anodes. Nanotechnology 24(42) (2013): 422001.
- [20] Harismah, K., Mirzaei, M., and Moradi, R. DFT studies of single lithium adsorption on coronene. Zeitschrift für Naturforschung A 73(8) (2018): 685-691.
- [21] Pattarapongdilok, N. and Parasuk, V. Adsorptions of lithium ion/atom and packing of Li ions on graphene quantum dots: Application for Li-ion battery. Computational and Theoretical Chemistry 1177 (2020): 112779.
- [22] Zheng, J., Ren, Z., Guo, P., Fang, L., and Fan, J. Diffusion of Li⁺ ion on graphene: A DFT study. Applied Surface Science 258(5) (2011): 1651-1655.
- [23] Wan, W., Zhang, Q., Cui, Y., and Wang, E. First principles study of lithium insertion in bulk silicon. Journal of Physics: Condensed Matter 22(41) (2010): 415501.

- [24] Tritsarlis, G.A., Zhao, K., Okeke, O.U., and Kaxiras, E. Diffusion of lithium in bulk amorphous silicon: a theoretical study. The Journal of Physical Chemistry C 116(42) (2012): 22212-22216.
- [25] Tritsarlis, G.A., Kaxiras, E., Meng, S., and Wang, E. Adsorption and diffusion of lithium on layered silicon for Li-ion storage. Nano Letters 13(5) (2013): 2258-2263.
- [26] Xu, S., Fan, X., Liu, J., Singh, D.J., Jiang, Q., and Zheng, W. Adsorption of Li on single-layer silicene for anodes of Li-ion batteries. Physical Chemistry Chemical Physics 20(13) (2018): 8887-8896.
- [27] Chinnathambi, S., Chen, S., Ganesan, S., and Hanagata, N. Silicon quantum dots for biological applications. Advanced healthcare materials 3(1) (2014): 10-29.
- [28] Cheng, X., et al. Enhancing quantum dots for bioimaging using advanced surface chemistry and advanced optical microscopy: application to silicon quantum dots (SiQDs). Advanced materials 27(40) (2015): 6144-6150.
- [29] Oda, S. Quantum dot devices: Technology vehicles for nanoscale physics and paths for future applications. in, pp. 333-336: IEEE.
- [30] Rani, P., Dalal, R., and Srivastava, S. Study of electronic and optical properties of quantum dots. Applied Nanoscience 12(7) (2022): 2127-2138.
- [31] Aghajamali, M., Xie, H., Javadi, M., Kalisvaart, W.P., Buriak, J.M., and Veinot, J.G.C. Size and surface effects of silicon nanocrystals in graphene aerogel composite anodes for lithium ion batteries. Chemistry of Materials 30(21) (2018): 7782-7792.
- [32] Choi, Y.-H., Park, H., Lee, S., and Jeong, H.-D. Synthesis and Electrochemical Performance of π -Conjugated Molecule Bridged Silicon Quantum Dot Cluster as Anode Material for Lithium-Ion Batteries. ACS omega 5(15) (2020): 8629-8637.
- [33] Zamfir, M.R., Nguyen, H.T., Moyen, E., Lee, Y.H., and Pribat, D. Silicon nanowires for Li-based battery anodes: a review. Journal of Materials Chemistry A 1(34) (2013): 9566-9586.
- [34] Peng, K., Jie, J., Zhang, W., and Lee, S.-T. Silicon nanowires for rechargeable lithium-ion battery anodes. Applied Physics Letters 93(3) (2008): 033105.

- [35] Shao, M., Ma, D.D.D., and Lee, S.T. Silicon nanowires–synthesis, properties, and applications. European Journal of Inorganic Chemistry 2010(27) (2010): 4264-4278.
- [36] Zhang, Q., Zhang, W., Wan, W., Cui, Y., and Wang, E. Lithium insertion in silicon nanowires: an ab initio study. Nano Letters 10(9) (2010): 3243-3249.
- [37] Salazar, F., Pérez, L.A., and Cruz-Irisson, M. Effects of surface passivation by lithium on the mechanical and electronic properties of silicon nanowires. Solid State Communications 247 (2016): 6-11.
- [38] De Santiago, F., et al. Lithiation effects on the structural and electronic properties of Si nanowires as a potential anode material. Energy Storage Materials 20 (2019): 438-445.
- [39] Du, C., Gao, C., Yin, G., Chen, M., and Wang, L. Facile fabrication of a nanoporous silicon electrode with superior stability for lithium ion batteries. Energy & Environmental Science 4(3) (2011): 1037-1042.
- [40] Yoo, J.-K., et al. Porous silicon nanowires for lithium rechargeable batteries. Nanotechnology 24(42) (2013): 424008.
- [41] Wada, T., Ichitsubo, T., Yubuta, K., Segawa, H., Yoshida, H., and Kato, H. Bulk-nanoporous-silicon negative electrode with extremely high cyclability for lithium-ion batteries prepared using a top-down process. Nano Letters 14(8) (2014): 4505-4510.
- [42] Wang, J., et al. Scalable synthesis of nanoporous silicon microparticles for highly cyclable lithium-ion batteries. Nano Research 13 (2020): 1558-1563.
- [43] Zhu, J., Gladden, C., Liu, N., Cui, Y., and Zhang, X. Nanoporous silicon networks as anodes for lithium ion batteries. Physical Chemistry Chemical Physics 15(2) (2013): 440-443.
- [44] González, I., Sosa, A.N., Trejo, A., Calvino, M., Miranda, A., and Cruz-Irisson, M. Lithium effect on the electronic properties of porous silicon for energy storage applications: a DFT study. Dalton Transactions 47(22) (2018): 7505-7514.
- [45] Young, D. Computational chemistry: a practical guide for applying techniques to real world problems. John Wiley & Sons, 2004.

- [46] Levine, I.N., Busch, D.H., and Shull, H. Quantum chemistry. Vol. 6: Pearson Prentice Hall Upper Saddle River, NJ, 2009.
- [47] Atkins, P., Atkins, P.W., and de Paula, J. Atkins' physical chemistry. Oxford university press, 2014.
- [48] Lewars, E. Computational chemistry. Introduction to the theory and applications of molecular and quantum mechanics 318 (2011).
- [49] Jensen, F. Introduction to computational chemistry. John wiley & sons, 2017.
- [50] Cramer, C.J. Essentials of computational chemistry: theories and models. John Wiley & Sons, 2013.
- [51] Fiolhais, C., Nogueira, F., and Marques, M.A.L. A primer in density functional theory. Vol. 620: Springer Science & Business Media, 2003.
- [52] Martin, J.M.L. and Santra, G. Empirical double-hybrid density functional theory: a 'third way' in between WFT and DFT. Israel Journal of Chemistry 60(8-9) (2020): 787-804.
- [53] Yoshio, M., Brodd, R.J., and Kozawa, A. Lithium-ion batteries. Vol. 1: Springer, 2009.
- [54] Olabi, A.G., Adil, M., Sayed, E.T., Iqbal, A., Rodriguez, C., and Abdelkareem, M.A. Lithium-ion batteries. in Reference Module in Materials Science and Materials Engineering 2021: Elsevier BV, 2020.
- [55] Biovia, D.S. Materials Studio. R2 (Dassault Systèmes BIOVIA, San Diego) (2017).
- [56] Betzinger, M., Friedrich, C., and Blügel, S. Hybrid functionals within the all-electron FLAPW method: implementation and applications of PBE0. Physical Review B 81(19) (2010): 195117.
- [57] Vilela Oliveira, D., Laun, J., Peintinger, M.F., and Bredow, T. BSSE-correction scheme for consistent gaussian basis sets of double- and triple-zeta valence with polarization quality for solid-state calculations. Journal of Computational Chemistry 40(27) (2019): 2364-2376.
- [58] Dovesi, R., et al. CRYSTAL17. (2017).

- [59] Xu, H., Yang, X.B., Guo, C.S., and Zhang, R.Q. An energetic stability predictor of hydrogen-terminated Si nanostructures. Applied Physics Letters 95(25) (2009): 253106.
- [60] Li, H., Xu, H., Shen, X., Han, K., Bi, Z., and Xu, R. Size-, electric-field-and frequency-dependent third-order nonlinear optical properties of hydrogenated silicon nanoclusters. Scientific Reports 6(1) (2016): 28067.
- [61] Zhao, Y. and Truhlar, D.G. The M06 suite of density functionals for main group thermochemistry, thermochemical kinetics, noncovalent interactions, excited states, and transition elements: two new functionals and systematic testing of four M06-class functionals and 12 other functionals. Theoretical chemistry accounts 120 (2008): 215-241.
- [62] Lipparini, F., et al. Gaussian 16 rev. A. O. Wallingford, CT (2016).
- [63] Petitjean, M. Spheres unions and intersections and some of their applications in molecular modeling. in Distance Geometry: Theory, Methods, and Applications, pp. 61-83: Springer, 2012.
- [64] Murray, J.S. and Politzer, P. In search of the 'impenetrable' volume of a molecule in a noncovalent complex. Molecular Physics 116(5-6) (2018): 570-577.
- [65] Hybertsen, M.S. and Louie, S.G. Electron correlation in semiconductors and insulators: Band gaps and quasiparticle energies. Physical Review B 34(8) (1986): 5390.

APPENDIX

Table A1. The change of molecular volume of various sizes of nLi-SiQDs

Si number	$\Delta MV \%$				
	Li-Td _{inner}	Li-Hex	Li-Td _{surface}	2Li-Td _{surface}	3Li-Td _{surface}
10	2.147	-	0.073	0.195	0.288
14	1.400	1.192	0.012	0.119	0.210
18	0.899	1.085	0.089	0.154	0.093
22	0.817	0.785	0.006	0.001	0.024
26	0.792	0.784	0.055	0.057	0.073
30	0.720	0.694	0.156	0.130	0.148
35	0.541	0.433	0.063	0.082	0.045
39	0.449	0.422	0.045	0.008	0.121
44	0.459	0.444	0.041	0.055	0.025
48	0.416	0.431	0.006	0.053	0.145

Table A2. The change of molecular volume after lithiation on SiNWs and SiNPs

a. Lithium absorbed and adsorbed on silicon nanowires (Li-SiNWs)

diameter (nm)	ΔMV (%)			
	Li-Td _{inner}	Li-Td _{surface}	2Li-Td _{surface}	3Li-Td _{surface}
1	0.495	0.27	0.157	0.158
1.5	0.258	0.138	0.045	0.095
2	0.164	0.099	0.003	0.091

b. Lithium absorbed and adsorbed on silicon nanopores (Li-SiNPs)

diameter (nm)	ΔMV (%)		
	Li-Td _{surface}	2Li-Td _{surface}	3Li-Td _{surface}
1	0.074	0.013	0.022
1.5	0.017	0.087	0.03
2	0.025	0.01	0.017

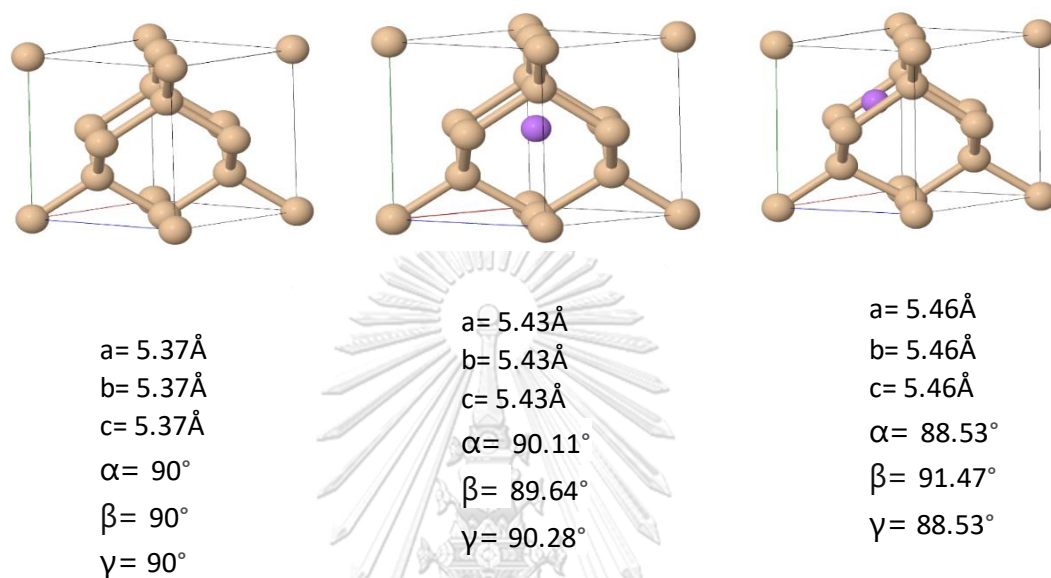
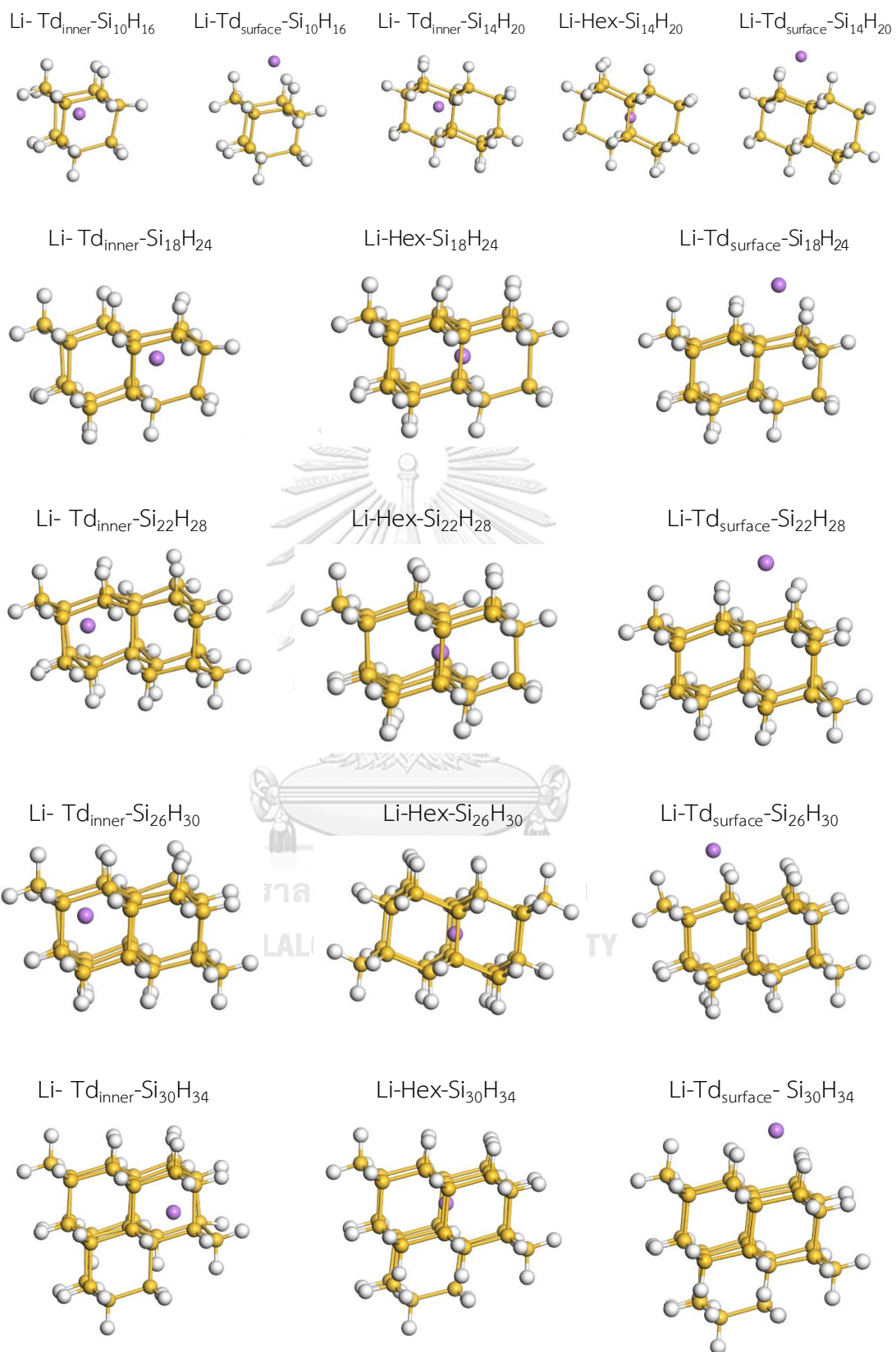


Figure A1. Optimized geometries of lithium absorption on bulk silicon (a) on tetrahedral (c) and hexagonal site (c)



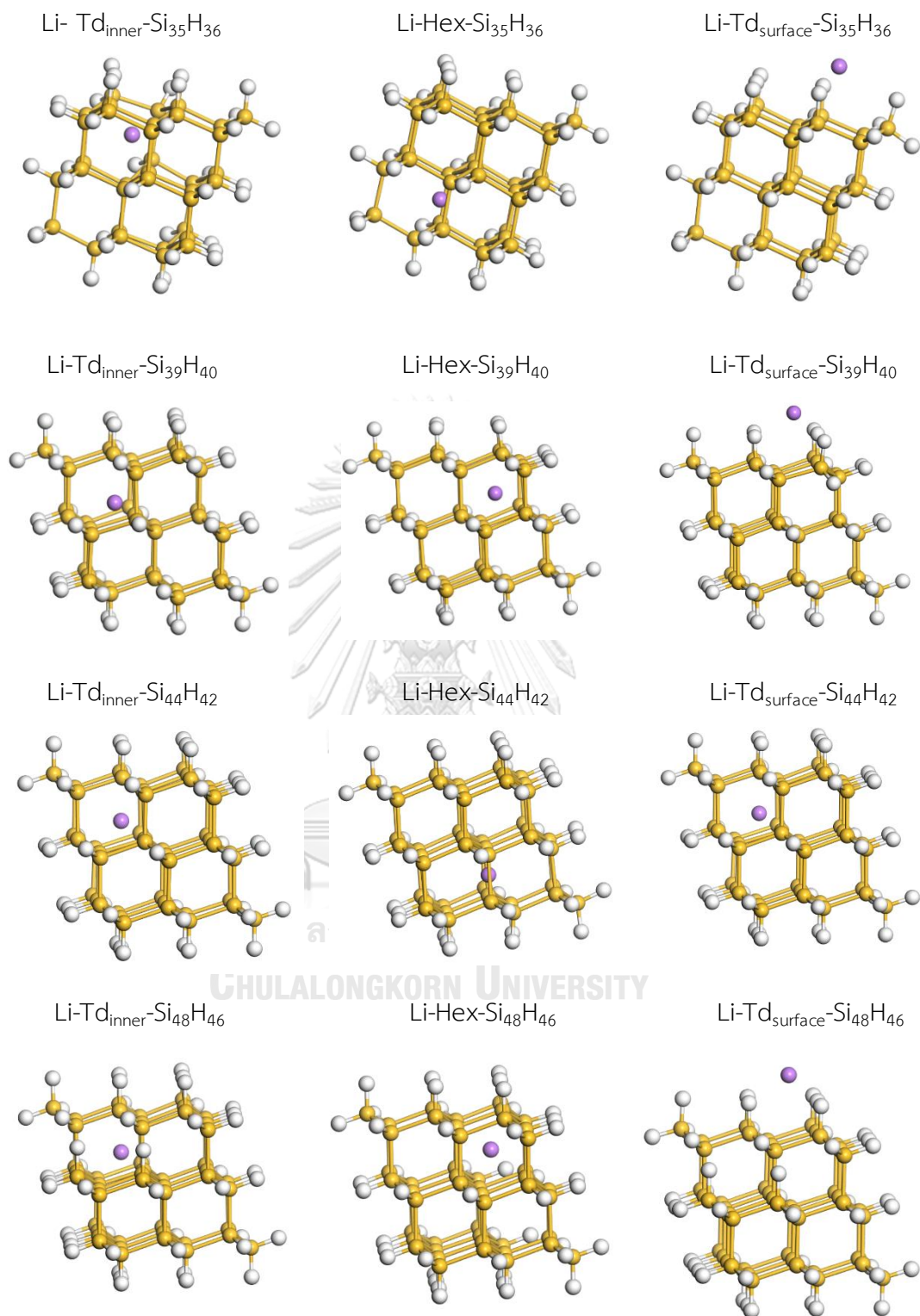
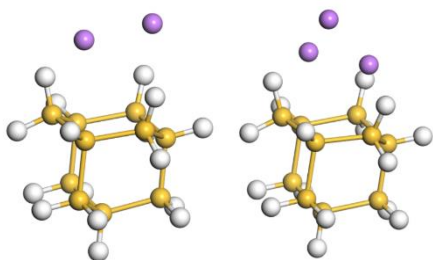
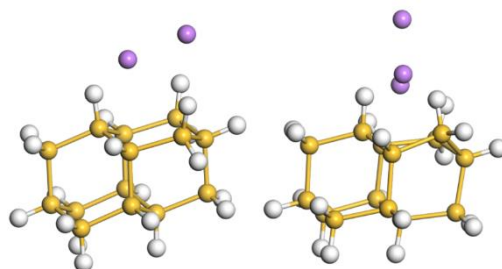
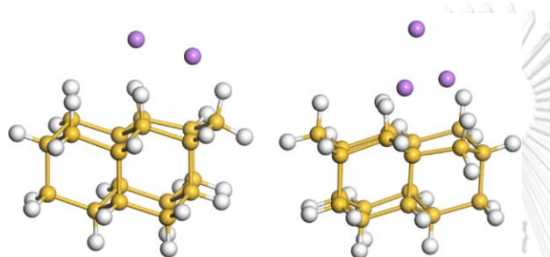
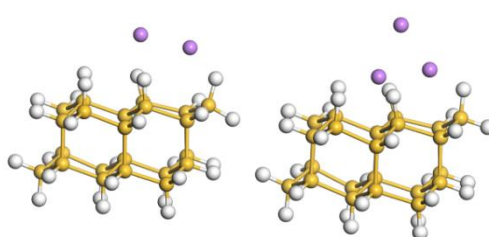
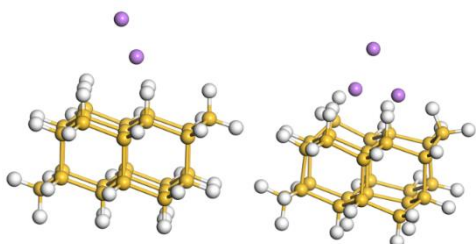
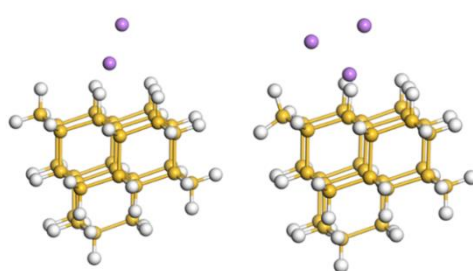
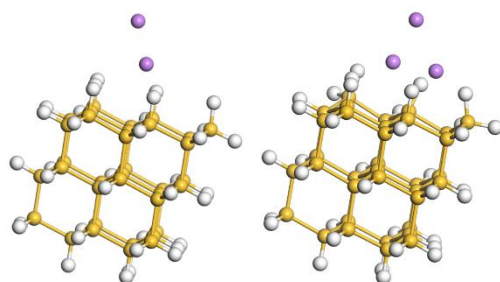
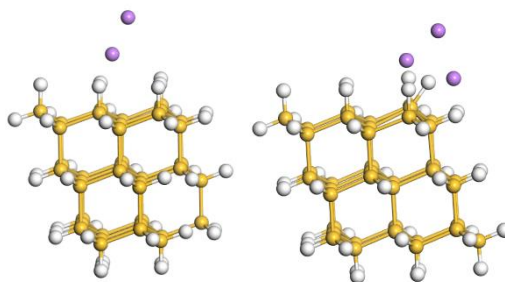
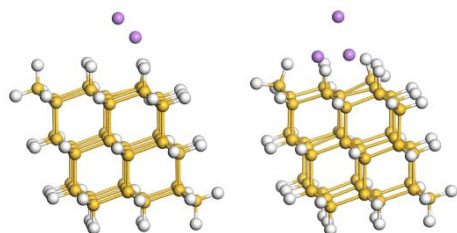


Figure A2. Optimized geometries of lithium absorption and adsorptions on SiQDs

2Li and 3Li adsorbed on $\text{Si}_{10}\text{H}_{16}$ 2Li and 3Li adsorbed on $\text{Si}_{14}\text{H}_{20}$ 2Li and 3Li adsorbed on $\text{Si}_{18}\text{H}_{24}$ 2Li and 3Li adsorbed on $\text{Si}_{22}\text{H}_{28}$ 2Li and 3Li adsorbed on $\text{Si}_{26}\text{H}_{30}$ 2Li and 3Li adsorbed on $\text{Si}_{30}\text{H}_{34}$ 2Li and 3Li adsorbed on $\text{Si}_{35}\text{H}_{36}$ 2Li and 3Li adsorbed on $\text{Si}_{39}\text{H}_{40}$ 

2Li and 3Li adsorbed on $\text{Si}_{44}\text{H}_{42}$



2Li and 3Li adsorbed on $\text{Si}_{48}\text{H}_{46}$

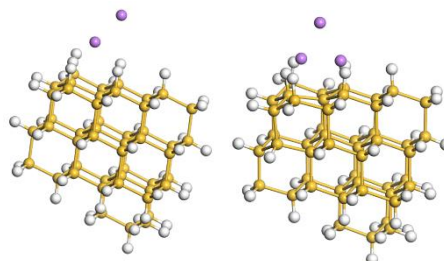


Figure A3. Second and third lithium adsorptions on SiQDs



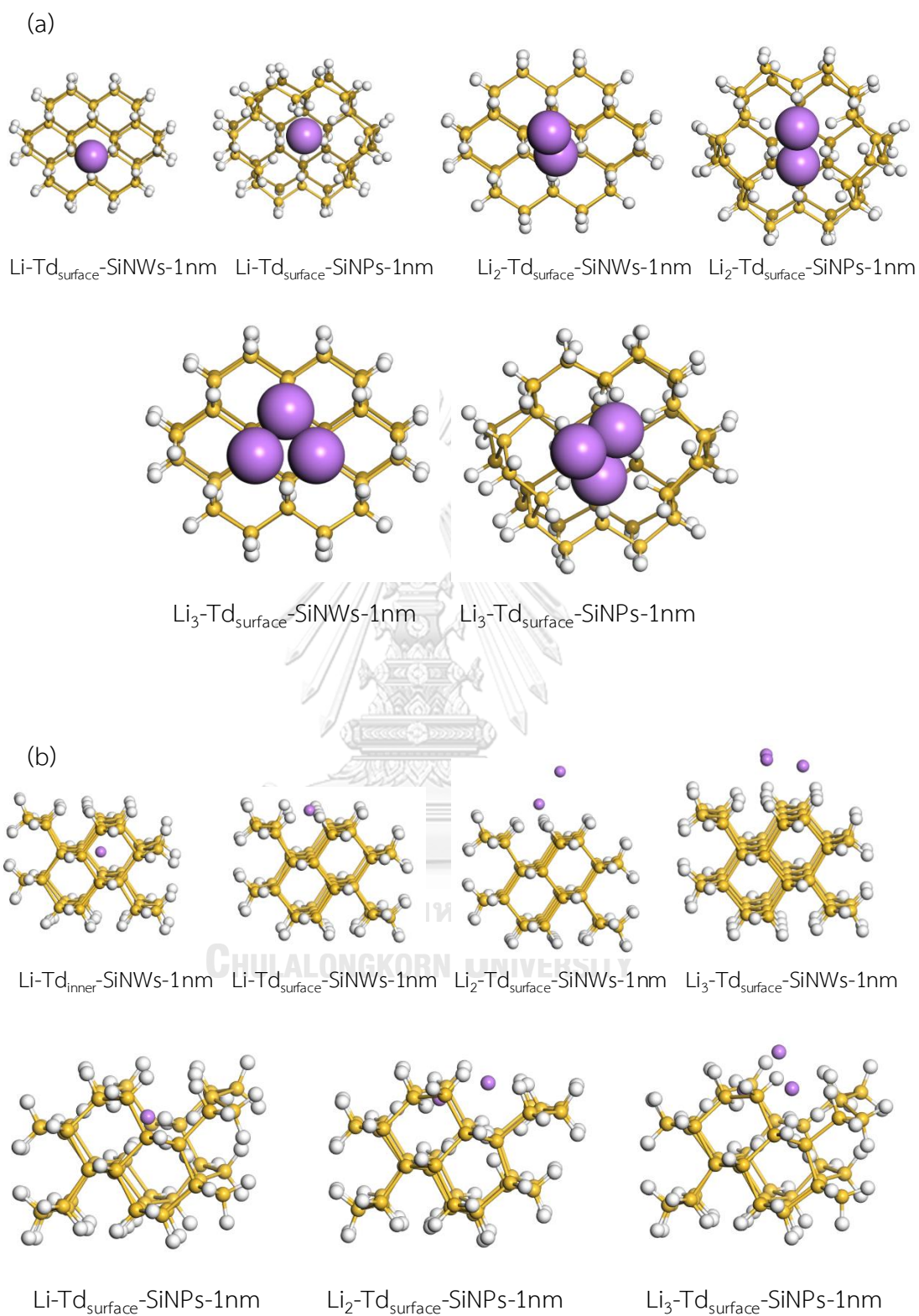


Figure A4. Optimized geometries of lithium absorption and adsorptions on silicon nanowires and nanopores, (a) top view and (b) side view

VITA

NAME Fadjar Mulya

DATE OF BIRTH 6 September 1993

PLACE OF BIRTH Jambi, Indonesia

INSTITUTIONS ATTENDED Bachelor of Science in Chemistry, Universitas Gadjah Mada, Indonesia
Master of Science in Chemistry, Chulalongkorn University, Thailand
Doctor of Philosophy in Chemistry, Chulalongkorn University, Thailand

HOME ADDRESS GKB 8th floor, Dr. Ir. H. Soekarno Road, Mulyorejo, Surabaya, Indonesia, 60215

PUBLICATION

1. Mulya, F., Santoso, G.A., Aziz, H.A. and Pranowo, H.D., 2016, July. Design a better metalloporphyrin semiconductor: A theoretical studies on the effect of substituents and central ions. In AIP Conference Proceedings (Vol. 1755, No. 1, p. 080006). AIP Publishing LLC.
2. Mulya, F. and Parasuk, V., 2020, February. Tetrachloroaluminate Ion on Graphene Quantum Dots: Towards the Design of Cathode for Aluminum-ion Battery. In Journal of Physics: Conference Series (Vol. 1463, No. 1, p. 012038). IOP Publishing.

AWARD RECEIVED Graduate scholarship programme for ASEAN or Non – ASEAN countries